DIRECTION-FINDING MEASUREMENTS OF TYPE III RADIO BURSTS OUT OF THE ECLIPTIC PLANE

by

Mark M. Baumback

A thesis submitted in partial fulfillment of the requirements for the degree of Master of Science in the Department of Physics and Astronomy in the Graduate College of The University of Iowa

May, 1976

Thesis supervisor: Professor Donald A. Gurnett

Graduate College
The University of Iowa
Iowa City, Iowa 52242

CERTIFICATE OF APPROVAL

MASTER'S THESIS

This is to certify that the Master's thesis of

Mark M. Baumback

has been approved by the Examining Committee for the thesis requirement for the degree of Master of Science in the Department of Physics and Astronomy at the May, 1976, graduation.

Thesis committee: Donald A. Gurnett
Thesis supervisor

Member

Member

ACKNOWLEDGMENTS

I wish to express my appreciation to R. West for his masterful work in the darkroom producing several of the figures and to the members of the Physics Drafting Department for their speed and advice in producing the figures for this thesis. I also thank S. Van Engelenhoven for her speed and efficiency in typing the manuscript, and to W. Kurth for his advice on the interpretation of the HAWKEYE 1 data. M. Montgomery provided plasma data from the Los Alamos plasma experiment on IMP 8. These data were very useful in establishing the local plasma densities necessary for the analysis. I am especially indebted to D. A. Gurnett for his guidance and support of the research described here.

This work was supported in part by the National Aeronautics and Space Administration under contracts NAS5-11431 and NAS1-13129 and Grant NGL-16-001-043 and by the Office of Naval Research under Grant N00014-76-C-0016.

ABSTRACT

Direction-finding measurements with the plasma wave experiments on the HAWKEYE 1 and IMP 8 satellites are used to find the interplanetary source locations of type III solar radio bursts in heliocentric latitude and longitude in a frequency range from 31.1 kHz to 500 kHz. Three events in the period from June 1974 to August 1974 were suitable to analyze completely. IMP 8 has its spin axis perpendicular to the ecliptic plane; hence, by analyzing the spin modulation of the received signals the location of the type III burst projected into the ecliptic plane can be found. HAWKEYE 1 has its spin axis nearly parallel to the ecliptic plane; hence, the location of the source out of the ecliptic plane can also be determined. Using an emperical model for the emission frequency as a function of radial distance from the sun the three-dimensional trajectory of the type III radio source can be determined from direction-finding measurements at different frequencies. If the electrons which produce these radio emissions are assumed to follow the magnetic field lines from the sun these measurements provide information on the three-dimensional structure of the magnetic field in the solar wind. The source locations projected into the ecliptic plane were found to follow an Archimedean spiral. Perpendicular to the ecliptic plane the source locations were found to usually follow a constant heliocentric latitude. When

the best fit magnetic field line through the source locations is extrapolated back to the sun this field line usually originates within a few degrees from the solar flare which produced the radio burst. With direction-finding measurements of this type it is also possible to determine the source size from the modulation factor of the received signals. For a type III event on June 8, 1974, the half angle source size was measured to be $\sim 60°$ at 500 kHz and $\sim 40°$ at 56.2 kHz as viewed from the sun.

TABLE OF CONTENTS

LIST OF TABLES

LIST OF FIGURES

I. INTRODUCTION

Broadband radio emissions of solar origin characterized by a rapid decrease in frequency with increasing time were reported by Wild and McCready [1950] and designated as type III radio bursts. These first observations of type III bursts were made in the frequency range from 70 to 130 MHz. In addition to being characterized by the rapid frequency drift, type III bursts have a lifetime which increases with decreasing frequency and have shorter rise times than decay times. The amplitude of the burst during the decay is proportional to e^{-kt} [Wild, 1950], where k is the decay constant and t is time. Ground based radio observations are limited to frequencies above about 10 MHz by the terrestrial ionosphere. For a general review of observations of type III radio bursts from the ground see Kundu [1965].

Wild *et al.* [1954] speculated that the rapid frequency drift is caused by charged particles moving outward through the solar corona emitting electromagnetic radiation at a frequency characteristic of the solar wind plasma density. Satellite measurements of energetic electrons emitted by solar flares confirm that these electrons generate the type III radio bursts. Solar flare electrons with energies of $\sim$ 40 keV were first observed in the interplanetary medium and identified to be of solar origin by Van Allen and Krimigis [1965]. A high correlation between the onset of solar flare electrons in the energy

range of 1 to 100 keV and type III emission near 1.0 AU indicates that these electrons generate the type III bursts [Lin, 1970; Alvarez et al., 1972; Frank and Gurnett, 1972; Lin et al., 1973; Alvarez et al., 1975; Gurnett and Frank, 1975].

Measurements of the frequency drift rates of type III bursts provide information on the solar wind density, if the frequency of emission as a function of heliocentric radial distance is assumed to be related to the local plasma frequency. The velocity of the exciter electrons may also be determined from the frequency drift rates. Exciter velocities ranging from 0.2 to 0.8 times the velocity of light, c, with an average velocity of 0.45 c were calculated for frequencies between 60 and 45 MHz [Wild et al., 1959]. The average exciter velocity calculated from measurements by the RAE 1 satellite for frequencies between 0.7 MHz and 2.8 MHz was 0.38 c [Fainberg and Stone, 1970]. Other drift rate measurements give similar results [Hartz, 1964; Hartz, 1969; Alexander et al., 1969; Haddock and Graedel, 1970; Fainberg and Stone, 1971]. These drift rate measurements give electron velocities that are in agreement with the energy range of the solar electrons observed in the interplanetary medium by the satellite experiments.

Ginzberg and Zhelezniakov [1958] suggested that type III bursts are generated by a coherent Cerenkov process. The energetic particles generate plasma waves at a frequency near the local plasma frequency by a two-stream instability. Then the plasma waves scatter off ion density inhomogeneities to produce electromagnetic radiation near the

plasma frequency and also scatter off other plasma waves to produce radiation near the second harmonic. The theory has since been revised but the process is basically the same [Smith, 1970, 1974]. To produce plasma waves more rapidly than they decay the energy distribution (velocity distribution) must have two peaks. Double peaked distributions associated with type III bursts have been observed with the IMP 7 and 8 satellites but plasma oscillations were seldom observed in association with solar electron events and type III bursts at 1.0 AU [Gurnett and Frank, 1975]. The measured electric field strengths of plasma oscillations are greater than the field strengths predicted by the current theories by approximately four orders of magnitude [Gurnett and Frank, 1975].

Models of the density of the solar wind can be used to determine the radial distances from the sun at which type III bursts radiate at different frequencies. Kaiser's [1975] study of the solar elongation of type III bursts indicates that the density of the solar wind from approximately 0.1 AU to 1.0 AU varies as $R^{-\gamma}$ where $2 \leq \gamma \leq 3$. Measurements of several thousand events were used to formulate the RAE emission level scale [Fainberg et al., 1972; Fainberg and Stone, 1974]. The RAE emission level scale relates the frequency of emission of a type III burst to the radial distance of the burst from the sun. A solar wind density model can be computed from the RAE emission level scale if it is assumed that the radiation occurs at the fundamental or second harmonic of the plasma frequency. Initially the radiation was assumed to be at the fundamental of the plasma frequency [Fainberg

et al., 1972]. For emission at the fundamental, the density $n_e = 5.52 \times 10^7 R^{-2.63}$ and the observed frequency $f_{obs} = 6.68 R^{-1.315}$ where R is the radial distance from the sun in solar radii, $R > 10R_\odot$, and f_{obs} is the observed frequency in megahertz. Alvarez and Haddock [1973] have obtained a similar density scale from type III observations where $n_e = N(\frac{214}{R-1})^{2.38}$. N is the plasma density at the earth and $R \geq 3.5 R_\odot$. The solar wind density models formulated from the analysis of type III bursts usually disagreed with the observed plasma densities at 1.0 AU [Newkirk, 1967] leading to the speculation that the bursts were generated along regions of enhanced density. However, density enhancements greater than a factor of 10 above the average density are rarely seen at 1.0 AU [Hundhausen, 1968]. Evidence now exists that radiation is predominantly at the second harmonic for low frequencies [Fainberg et al., 1972; Fainberg and Stone, 1974; Lin et al., 1973; Haddock and Alvarez, 1973; Alvarez et al., 1975; Kaiser, 1975].

At frequencies greater than several megahertz, type III radiation is predominantly at the fundamental of the plasma frequency. However some bursts are observed to radiate in narrow bands at the fundamental and second harmonic of the plasma frequency. The frequency ratio of the second harmonic to the fundamental in the majority of events lies between 1.85 and 2.00 [Wild et al., 1954; Kundu, 1965]. A ratio of less than 2.00 is probably cuased by the sharp cutoff below the plasma frequency, allowing only the high frequency portion of the fundamental band to propagate. Haddock and Alvarez [1973] report that near 1 MHz the radiation appears to shift from predominantly

fundamental to predominantly second harmonic radiation. The assumption of second harmonic emission brings densities calculated from the RAE emission level scale to better agreement with solar wind density measurements at 1.0 AU. For a model of the solar wind plasma density this paper uses the RAE emission level scale with the assumption of second harmonic emission. For a review of density measurements see Newkirk [1967].

The first satellite observations of type III bursts were made by Hartz [1964] with a receiver on the Alouette 1 spacecraft. With satellite observations it is possible to detect type III bursts down to frequencies of near the solar wind plasma frequency, which is typically about 25 kHz at 1.0 AU. The lowest frequency at which a type III burst has ever been observed is 10 kHz [Kellogg et al., 1973].

Satellite observations of type III bursts at hectometric wavelengths (frequencies between 0.3 and 3.0 MHz) usually, but not always, correlate with ground based observations of type III bursts at decametric wavelengths (frequencies between 3.0 and 30 MHz). More decametric bursts are reported than hectometric bursts, possibly due to the higher sensitivities of the ground based receivers. However, cases have been reported of high intensity bursts at lower frequencies that are weak or entirely absent at higher frequencies [Hartz, 1969; Fainberg and Stone, 1970a].

If the electrons that generate type III bursts are assumed to travel along the solar magnetic field lines, information can be obtained about the structure of the interplanetary magnetic field by

analyzing the direction of arrival of a type III burst as a function of frequency. The source location, the region of interplanetary space where the type III radio emission is generated at a particular frequency, can be determined from the direction-finding measurements and the radial distance of the emission from the sun, computed from a model of the solar wind density. The source locations of the burst as a function of frequency, and hence radial distance, trace the magnetic field out from the sun.

The first direction-finding measurements of type III bursts were made by Slysh [1967] using spin modulation and lunar occultations of the Luna 11 and 12 satellites to determine the source locations. Direction-finding measurements on the IMP 6 spacecraft confirmed that the type III emission regions as a function of frequency, and hence the electrons generating the type III bursts, follow the Archimedean spiral structure of the interplanetary solar magnetic field [Lin et al., 1973; Fainberg et al., 1972; Fainberg and Stone, 1974; Stone, 1974].

Up to the present time direction-finding measurements of type III radio bursts have provided only one coordinate, in the plane of rotation of the antenna, of the direction of arrival. These one-dimensional measurements therefore only give a projection of the source location and do not provide a unique determination of the trajectory of the radio burst. Measurements of the source size from the spin modulation are similarly ambiguous for such one-dimensional measurements since the modulation factor of the received signal is a

function of the unknown elevation angle of the source above the plane of rotation of the antenna.

The purpose of this paper is to present a series of two-dimensional direction-finding measurements of type III radio bursts using spin modulation measurements from two satellites (IMP 8 and HAWKEYE 1) which have their spin axes nearly perpendicular to each other. Simultaneous direction-finding measurements from these satellites provide a unique determination of the direction of arrival (along a line) and the angular size of the source. This two-dimensional direction-finding technique is used, together with a model for the solar wind plasma density, to provide determinations of type III source locations out of the ecliptic plane and information on the three-dimensional structure of the solar magnetic field at radial distances of 0.2 to 1.0 AU from the sun.

II. DESCRIPTION OF INSTRUMENTATION

Data from two satellites, IMP 8 and HAWKEYE 1, are used in the direction finding analysis. To determine the source locations of the type III bursts the spin modulation of the observed signal intensity was analyzed to determine the apparent direction to the type III source. All of the data presented in this paper were taken while the satellites were in the solar wind. Therefore, it was possible to analyze the events to frequencies near the solar wind plasma frequency, which is typically about 25 kHz at 1.0 AU.

A. IMP 8

The IMP 8 spacecraft was launched into earth orbit from the Eastern Test Range on October 26, 1973. The orbit is slightly eccentric with initial perigee and apogee geocentric radial distances of 147,434 km and 295,054 km respectively, orbit inclination of 28.6°, and a period of 11.98 days. The spacecraft is spin stabilized with its spin axis oriented very nearly perpendicular to the ecliptic plane, and has a spin period of about 2.59 sec. Figure 1 qualitatively shows the IMP 8 orbit.

The University of Iowa plasma wave exeriment on IMP 8 measures the average electric field intensity in a frequency range from 40 Hz to 2 MHz and the average magnetic field intensity from 40 Hz to 1.78 kHz. The electric field receiver is connected to a dipole antenna

with a nominal tip-to-tip length of 121.8 meters extended perpendicular to the spin axis, and the magnetic field receiver is connected to triaxial search coil magnetometer.

In the range from 40 Hz to 1.78 kHz two identical seven channel spectrum analyzers measure the peak and average intensities for both electric and magnetic fields with a dynamic range of 120 db. The effective noise bandwidths for each channel are ± 15% except for the 40 Hz channels which are ± 30%. Each channel of the spectrum analyzers is sampled every 10.24 sec. The input voltages are compressed by a circuit, a logarithmic compressor, which provides an output voltage proportional to the logarithm of the input voltage.

In the frequency range from 5.6 kHz to 178 kHz an eight channel step frequency receiver with an effective noise bandwidth of ± 7.5% for each channel measures the average electric field intensity with a dynamic range of 100 db. Each step frequency receiver channel output is sampled every 10.24 seconds.

A tunable wideband receiver, with approximately 100 db of dynamic range, measures the average electric or magnetic field intensity from zero to one kHz or the electric field intensity at 31.1 kHz, 125 kHz, 500 kHz, or 2 MHz with a bandwidth of ± 1 kHz. The wideband receiver provides intensity measurements every 1.28 seconds.

B. HAWKEYE 1

The HAWKEYE 1 spacecraft was launched into polar earth orbit on June 3, 1974, from the Western Test Range. The orbit is highly eccentric with initial perigee and apogee geocentric radial distances

of 6847 km and 130,856 km respectively, inclination of 89.79° to the equator and period of 49.94 hours. The initial argument of perigee is 274.6°; thus apogee is almost directly over the north pole. The spacecraft is spin stabilized with a spin period of about 11.0 sec. The spin axis lies in the plane of the orbit and is nearly parallel to the equatorial plane with a right ascension of 300.7° and declination of 6.8°. Figure 2 shows qualitatively the HAWKEYE 1 orbit.

The HAWKEYE 1 plasma wave experiment is similar to the IMP 8 plasma wave experiment. This experiment measures the electric field intensity in a range from 1.78 Hz to 178 kHz, and the magnetic field intensity in a range from 1.78 Hz to 5.62 kHz. The electric field receiver is connected to a dipole antenna with a nominal tip-to-tip length of 42.45 meters, extended perpendicular to the spin axis. The magnetic field receiver is connected to a search coil magnetometer that is oriented parallel to the spin axis.

The eight lower frequency channels, 1.78 Hz to 5.62 kHz, alternately measure the electric and magnetic field intensities every 23.04 seconds. The upper eight frequency channels, 13.3 kHz to 178 kHz, measure the electric field intensity every 11.52 seconds. The output voltages are proportional to the logarithm of the input voltage.

In addition to the digital outputs from the spectrum analyzer described above, the experiment has a wideband analog output with selectable bandwidths of 10 kHz or 45 kHz. Either electric or magnetic antennas can be switched to the wideband receiver. The

wideband receiver is automatic-gain controlled (AGC) to provide good amplitude resolution over a given spectrum with large dynamic range.

This paper is concerned primarily with the HAWKEYE 1 and IMP 8 electric field data in the range of 31.1 kHz to 500 kHz.

III. DIRECTION FINDING TECHNIQUE

A. Method of Analysis

A rotating dipole antenna pattern provides a simple method of determining the direction to a source of electromagnetic radiation. The amplitude of the detected signal is a function of the angle between the source and the antenna axis. As the dipole antenna rotates the signal is modulated, with a null in the modulation pattern occurring when the antenna is most nearly parallel to the propagation vector and a maximum when the antenna axis is perpendicular to the propagation vector. The depth of the null is determined by the size of the source and the elevation angle, α, between the plane of rotation of the antenna and the direction to the source. As α increases or as the source size increases the depth of the null decreases. Figure 3 shows the spin modulated pattern with a one hour averaging period for the IMP 8 178 kHz channel during one of the type III events analyzed. The normalized field strength is plotted as a function of the orientation angle δ_y, the angle between the +y antenna and the spacecraft-sun line projected into the spacecraft spin plane. (Figures 1 and 2 define the angle δ_y for both HAWKEYE 1 and IMP 8.) Each point represents the average of the normalized field strengths which have been accumulated in each 10° angle bin. The angle δ, at which the null occurs, is computed by a least squares fit of the

normalized field strengths, as a function of δ_y, to the theoretical modulation pattern.

For both HAWKEYE 1 and IMP 8 the interval between samples is greater than the spin period; thus, many rotations of the satellite are required to obtain a uniform angular distribution of samples through 360°. HAWKEYE 1 rotates through 360° plust about 17° between consecutive samples so that on the order of 21 rotations of the satellite are required to obtain a uniform distribution of samples through 360°. IMP 8 rotates through four rotations minus about 19° between consecutive samples so that on the order of 75 rotations of the satellite are required to sample uniformly through 360°. The period of time necessary to sample uniformly through 360° will be referred to as a sampling cycle. For both HAWKEYE 1 and IMP 8 a sampling cycle is approximately 3 or 4 minutes.

The direction-finding routines used for analysis normalize the data to reduce the effects of amplitude changes that take place in a time interval that is long compared to the spin period. This normalization is performed by subtracting the average of all samples in the sampling cycle from each of the individual samples. Since the samples are proportional to the logarithm of the electric field intensity the normalization process is equivalent to dividing each sample by the geometric mean intensity during the sampling cycle. The normalized samples taken over many of the sampling cycles are sorted into 10° angle bins and the normalized samples within each bin are averaged. Since the dipole pattern is assumed to be symmetric

the data from $90° < \delta_y \leq 270°$ are shifted into the range from $-90° < \delta_y \leq 90°$ by subtracting 180°.

For the IMP 8 data two direction-finding methods are used. The first method accumulates the normalized samples in the 10° bins for the entire analysis period. When the analysis period has ended the normalized samples are averaged within the 10° bins, each normalized sample receiving an equal weighting. The analysis period for this method usually will last from 30 minutes to several hours, depending upon the duration of the event. This method is used for determining the least squares fit δ over the duration of the event. The second direction-finding routine computes the null direction averaged over 10 minute intervals, rather than the average null direction for the entire event. This method averages the normalized samples within each 10° bin at the end of each sampling cycle. For averaging, samples from different sampling cycles are weighted differently. The weighting factor for a normalized sample from the i^{th} sampling cycle is $e^{-(t-t_i)/\lambda}$, where λ is the time constant, t_i is the time associated with the i^{th} sampling cycle and t is the time associated with the current sampling cycle. Thus the newly acquired samples have a weighting factor of 1 while the previous samples have a weighting factor which decreases exponentially for earlier times. The time constant used for the analysis in this paper is 10 minutes. δ is computed from the averages in the 10° bins approximately every 6 minutes. This method of analysis is used in order to study changes in the direction of arrival during the event, and aids in choosing the analysis period for the first method.

The HAWKEYE 1 data were analyzed by accumulating normalized samples in 10° bins for the entire analysis period. When the analysis period has ended the normalized samples within each 10° bin are averaged, each normalized sample having an equal weighting. δ is computed at the end of the analysis period. The analysis period usually covered the duration of the event. To aid in choosing the analysis period the program was run for 10 minute averaging periods, computing δ at the end of each averaging period.

For both HAWKEYE 1 and IMP 8 an accurate determination of δ is found by doing a least squares fit of the normalized field strengths E/E_o to the theoretical expression for the modulation envelope given by

$$\left(\frac{E}{E_o}\right)^2 = \left(1 - \frac{m}{2}\right) - \frac{m}{2} \cos\left[2(\delta_y - \delta)\right] \qquad (1)$$

where E/E_o is the normalized intensity and δ_y is the orientation angle of the electric antenna axis in the plane of rotation of the antenna. The null direction, δ, is the direction to the centroid of the source projected into the spin plane of the antenna. The modulation factor, m, provides a quantitative measure of the null depth: m is zero for no spin modulation, and m is one for the maximum modulation. The null direction computed represents the least squares fit δ over the duration of the event. δ_y is computed from the optical aspect data and the receiver time constants. The receiver time constant correction for HAWKEYE 1 is $1.3° \pm .2°$ and for IMP 8 is $11.96° \pm 2°$. The time constant correction angle is found by calculating the angle through

which the spacecrafts rotate in one time constant of the receiver. δ_y is thus the angle at which the antennas are physically oriented with respect to the sun minus the time constant correction angle.

B. Geometry in the Analysis

The null direction computed from each satellite locates a plane in which the source must lie. The source location lies along the intersection of the source planes determined by the two satellites. Figure 4 defines the geometry of the source planes and the angles and vectors used for the computation of the source location. The spin plane is the plane in which the antenna rotate. The spin axis, $\vec{S}$, is perpendicular to the spin plane. The source plane is the plane in which both the spin axis of the satellite and the source lie. The angle between the satellite-sun line projected into the spin plane and the intersection between the spin plane and the source plane is δ. Normals to both source planes are constructed. $\hat{n}_1$ is normal to IMP 8's source plane and $\hat{n}_2$ is normal to HAWKEYE 1's source plane. The source direction vector is given by $\hat{n}_1 \times \hat{n}_2$. There is, however, a 180° ambiguity in the source location. At high frequencies this ambiguity is decided by assuming that the source is in the direction toward the sun. At lower frequencies, where the source could be located at radial distances beyond 1.0 AU if the emission is at the second harmonic of the plasma frequency, the ambiguity is decided by requiring the source position to be in agreement with an extrapolation of the measurements at higher frequencies. The source direction computed from $\hat{n}_1 \times \hat{n}_2$, after deciding the ambiguity, is given in Geocentric Solar

Ecliptic coordinates, λ_{GSE} and φ_{GSE}. The angle λ_{GSE} is the Geocentric Solar Ecliptic latitude of the source, measured positive northward from the ecliptic plane. The angle φ_{GSE} is the Geocentric Solar Ecliptic longitude of the source, measured positive counterclockwise from the satellite-sun line as viewed from the north ecliptic pole. Since the IMP 8 spin axis is perpendicular to the ecliptic plane the null angle δ, which is referenced to the sun direction, is identical to the Geocentric Solar Ecliptic longitude of the source. The source location at a particular frequency is determined by the intersection of the source direction vector, $\hat{n}_1 \times \hat{n}_2$, with a sphere centered on the sun with a radius equal to the radial distance from the sun of the type III emission.

C. Possible Errors in Analysis

The accurate determination of δ and the modulation are dependent upon a number of considerations. First the data must not be contaminated with sources other than the type III bursts. A high percentage of the time Auroral Kilometric Radiation (AKR) from the earth is seen by one of both satellites. IMP 8 detects AKR for approximately 42% of the time in the 178 kHz channel. HAWKEYE 1 detects AKR for 60% of the time in the 178 kHz channel [Green, personal communication, 1975]. This considerably reduces the number of events that can be analyzed. Second, at predominantly the lower frequencies, δ changes over a fairly wide range of angles during the type III event. The δ used in the analysis is computed over the

duration of the event and represents a least squares fit δ for the duration of the event. Third, when the modulation factor is low, the determination of δ is sensitive to changes in amplitude of the radiation during the event and to noise spikes unrelated to the type III event. The noise spikes should not be used in the analysis to determine δ. When the modulation factor is low the quantizing steps of the spacecraft analog to digital converter also reduces the accuracy in computing δ. The errors due to a low modulation factor affect primarily the 56.2 kHz, 42.2 kHz and 31.1 kHz channels. Fourth, the polarization of the radiation may cause errors in the determination of δ. If the source position were collinear with the spin axis, the null angle would correspond directly to the smallest transverse electric field vector. A randomly or circular polarized source will produce no error due to polarization. A polarized source in the spin plane will also produce no error due to polarization. For IMP 8 measurements the source is usually near the spin plane, which minimizes polarization errors.

IV. CHARACTERISTICS OF TYPE III BURSTS AT LOW FREQUENCIES

At low frequencies the type III bursts have several readily observed characteristics. Some of the characteristics are observed at high frequencies, while other characteristics are observed predominantly at the lowest frequencies. These characteristics are illustrated by the events shown in Figures 5 to 9.

A. Frequency Drift Rates

Type III bursts are characterized by a rapid drift in frequency with time. The higher frequencies are observed first, followed by the lower frequencies. The drift rates can be measured from the burst onset times at each of the frequencies or from the time for the peak amplitude of the burst at each of the frequencies. Figure 5 shows a type III event observed simultaneously by both IMP 8 and HAWKEYE 1. This figure is a plot of the logarithm of the electric field intensity measured by the plasma wave experiments on board the two satellites. The data from seven frequency channels of each experiment are displayed as a function of time. Notice that in addition to a type III event, other naturally occurring radio signals such as auroral kilometric radiation and magnetosheath electrostatic noise are observed. The characteristic frequency drift is evident in the type III event shown in Figure 5.

On an individual basis the measurement of drift rates yields little information other than the exciter speed. If the electrons have a non zero pitch angle then the path of the electrons is longer than the distance along the spiral to the sun and the exciter speed will not correspond to the electron energy. Lin [1974] reports that electrons have appreciable pitch angles at 1.0 AU and that the total path travelled is longer than the average spiral path.

B. Burst Rise and Decay Times

For an individual frequency the amplitude rises quickly with increasing time followed with a much slower exponential decay [Kundu, 1965]. The decay time increases with decreasing frequency. At frequencies of several hundred megahertz the burst duration is on the order of seconds, while at the lowest observable frequencies (tens of kilohertz) the burst duration is several hours. Figures 6 through 9 show type III bursts at frequencies of 500 kHz, 178 kHz, 100 kHz and 56.2 kHz. The burst duration at 500 kHz is approximately 20 minutes (Figure 6) while at 56.2 kHz (Figure 9) the burst lasts for more than 4 hours. Since the logarithm of the burst's amplitude is plotted as a function of time, the exponential decay is a straight line. The exponential decay is very clear in the 100 kHz (Figure 8) and 56.2 kHz (Figure 9) channels.

C. Modulation Factor of Type III Bursts

The modulation factor of the burst varies with frequency and time. The modulation factor at a particular frequency is usually

greater near the start of the burst than near the end of the burst. The modulation factor also decreases with decreasing frequency. At 500 kHz the modulation is usually greater than 0.80 while at frequencies on the order of the local plasma frequency at 1.0 AU the modulation disappears completely. In the top panel of Figures 6 to 9 the logarithm of the electric field intensity is plotted as a function of time. The modulation of the received electric field intensity caused by the rotation of the dipole antenna is seen as a periodic amplitude fluctuation with a periodicity of about 100 sec., one half of the beat period between the sampling rate and the spin period. The bottom panels of Figures 6 to 9 display the modulation factor calculated from Eq. (1) as a function of time. The modulation factor for the burst shown in Figure 6 at 500 kHz is .80 near the start of the burst but then drops to .70 near the end of the event. For the burst shown in Figure 7 at 178 kHz the modulation factor is approximately .75 near the start, but then drops to slightly greater than .5 near the end of the burst. For the burst shown in Figure 8 at 100 kHz the modulation factor at the start of the burst is about 0.65 while near the end of the burst the modulation factor is about 0.25. The burst shown in Figure 9 at 56.2 kHz is very near to the earth and has a very large source size, and thus has no modulation.

D. Variations in Direction of Arrival During Type III Bursts

The direction of arrival is observed to vary in time for any one frequency. At a particular frequency the direction of arrival changes systematically during the duration of the burst, usually

starting near the sun and deviating away from the sun later in the event. The direction of arrival usually varies over a wider range at the lower frequencies. At 500 kHz (Figure 6) there is a shift in the φ_{GSE} of the source of about 10°. The position of the earth is also shown to aid in the identification of AKR and other terrestrial sources which may contaminate the signal from the type III burst. At 178 kHz (Figure 7) there is a shift in φ_{GSE} of the sources of approximately 25°. A highly modulated source of terrestrial origin is present before and after the type III burst. At 100 kHz (Figure 8) φ_{GSE} is initially near 0° (in the direction of the sun), but then changes to approximately 45° at the end of the event. Since the burst shown in Figure 9 at 56.2 kHz has no spin modulation the slope of the rise and decay positions of the event dominates in the direction finding analysis and produces incorrect longitude for this example. The direction of arrival for a burst cannot be determined if the modulation factor is too small. To compute the source locations for the events analyzed in this paper, the direction of arrival is the least squares fit δ computed over the duration of the event.

V. PLASMA DENSITY AND SOLAR MAGNETIC FIELD MODELS

Models of the solar wind density and the solar magnetic field are necessary to determine the source locations of the type III burst in three dimensions. Since data from only two satellites are used in the analysis, only two components of the source locations can be determined. A model of the solar wind plasma density provides the information required to determine the third component of the source locations.

A. RAE Emission Level Scale

The frequency of emission of type III bursts is a function of solar wind density; therefore, if a density scale of the solar wind as a function of heliocentric radial distance is assumed, it is possible to calculate the distance from the sun to the type III burst emission region. The RAE emission level scale [Fainberg and Stone, 1970b, 1974; Fainberg et al., 1972] gives the frequency of emission as a function of heliocentric radial distance.

Fainberg and Stone [1970b] analyzed the burst drift rates of several thousand type III bursts observed by the RAE I satellite to determine an average density scale for the solar wind. The burst drift time, the time delay between emission at two frequencies, shows a dependence on the heliocentric longitude of the associated active

region [Fainberg and Stone, 1970b]. The drift time depends not only on the time required for the exciter particles to travel between the plasma levels but also depends upon the propagation times from the two source regions to the observer. A least squares analysis of the RAE data provides the best fit values of the separation between plasma levels and also provides the average exciter velocity between the plasma levels. The heliocentric radial distance to the emission level for the source nearest the sun (the higher frequency source) was assumed in Fainberg and Stone's analysis; however later a self consistent method based on the emission level separations was used to determine the heliocentric radial distance to the emission level for the source nearest the sun. By combining the results from the drift rate analysis for a wide range of frequencies the RAE emission level scale was computed. Fainberg and Stone's [1970b] analysis determined the average heliocentric radial distance of a type III source location as a function of frequency, independent of any assumptions about the solar wind density. A density scale as a function of heliocentric radial distance for the solar wind can be computed by assuming that the frequency of emission is at either the plasma frequency or at a harmonic of the plasma frequency. The density scale shown in Figure 10 is based on the RAE emission level scale and assumes emission at the second harmonic of the plasma frequency. The plasma density scale agrees more closely to the average in situ measurements of the density at 1.0 AU if second harmonic emission is assumed.

Since the RAE emission level scale is an average of many thousands of bursts, it is desirable on an individual basis to adjust the RAE emission level scale so that the density scale agrees with the plasma density measured at 1.0 AU in the solar wind. When the trajectory of the exciter electrons passes near the earth and in situ measurements of the solar wind density are available, the RAE emission level scale is adjusted to agree with the in situ density measurements.

B. Models of the Solar Magnetic Field

1. Solar Magnetic Field Line Configuration in the Ecliptic Plane

In the interplanetary medium the magnetic fields are constrained to move with the solar wind plasma flow. For the simplest model the solar wind plasma flows radially out of the sun at a constant velocity of approximately 400 km sec^{-1}. Since the sun is rotating the resulting magnetic field projected into the ecliptic plane corresponds to an Archimedean spiral [Parker, 1963, 1964, 1965]. Measurements in the ecliptic plane confirm the general spiral structure of the magnetic field [Schatten et al., 1968; and review by Schatten, 1972]; however, the magnetic field is usually distorted from a perfect spiral configuration. For example, changes in the velocity of the solar wind will produce kinks in the spirals. Other distortions may be caused by variations in the magnetic field near the sun and by magnetic field loops in which the field lines near the sun reconnect back to the sun [Schatten, 1972]. The solar magnetic field has a sector structure in which the magnetic field is predominantly inward or outward in adjacent sectors [Schatten, 1968; Wilcox and Ness, 1967].

The sector pattern has a 27 day periodicity related to the 27 day rotation period of the sun as viewed from earth. Evolution of the sector structure can be observed in consecutive rotations of the sun [Schatten, 1968].

2. Solar Magnetic Field Line Structure in the Meridian Plane

No direct measurements have been made of the solar magnetic field configuration out of the ecliptic plane, in the interplanetary medium. The structure of the solar magnetic field may be deduced by indirect measurements, such as the analysis of type III bursts, because the trajectory of the electrons that generate type III bursts is along the solar magnetic field lines.

a. Constant Latitude Model. The simplest model of the solar magnetic field out of the ecliptic plane is the constant latitude model shown in Figure 11, which corresponds to a uniform radial flow of the solar wind plasma away from the sun. Projected into the ecliptic plane the field lines are Archimedean spirals, while in a meridian plane the magnetic field lines are at a constant latitude. The constant latitude model corresponds to Archimedean spirals wound on cones of constant heliocentric latitudes.

b. Convergent Field Line Model. The structure of the solar corona photographed during solar eclipses indicates that high latitude polar fields may extend to low latitudes at 1.0 AU [Schatten, 1972]. The convergent field line model shown in Figure 11 is suggested by these observations. For this model the solar magnetic field projected

into the ecliptic plane follows the Archimedean spiral but in the meridian plane the magnetic field lines extend to lower heliocentric latitudes with increasing radial distances.

c. Divergent Field Line Model. Magnetic field measurements near 1.0 AU show a consistent skewing of the magnetic field away from the equatorial plane [Coleman and Rosenberg, 1971; Rosenberg and Winge, 1974]. Such skewing may be caused by magnetic field diffusion in the interplanetary medium [Schatten, 1972]. Stream interactions may contribute to an azimuthal velocity component in the solar wind or to a net divergence of mass and magnetic flux away from the equatorial plane [Suess et al., 1975]. The divergence of the magnetic field away from the equator could also be caused by magnetic pressure. The magnetic field spiral angle and, therefore, the magnetic pressure changes with heliocentric latitude. The magnetic pressure is greatest near the equator, causing mass and magnetic flux to be carried away from the equatorial plane [Suess, 1974; Suess and Nerney, 1975]. These observations suggest the divergent field line model shown in Figure 11. In this model the magnetic field projected into the ecliptic plane follows an Archimedean spiral, but in the meridian plane the magnetic field lines extend to higher heliocentric latitudes with increasing radial distances.

Coronal photographs and in situ measurements of the solar magnetic field each suggest different models of the solar magnetic field. It may be possible to more accurately determine the actual solar magnetic field structure by tracking the trajectories of the exciter particles of type III bursts.

VI. ANALYSIS OF EVENTS

Twenty events were initially chosen from the first 43 orbits of HAWKEYE 1 and from the same time period for IMP 8 to analyze. However of the initial 20 events only three events were analyzed completely. Events were thrown out for several reasons. First, some of the bursts were thrown out because they were actually multiple bursts originating from different regions of the sun. When there is electromagnetic radiation coming from two different sources the direction-finding analysis cannot resolve the separate sources, but gives the average of the two source locations. Second, where there might be good frequency coverage from one satellite, the data from the other satellite would not have adequate coverage. Third, even when there was good coverage on both of the satellites some of the bursts had to be thrown out because there were large errors in determining the source location of the burst, caused by Auroral Kilometric Radiation and other sources contaminating the type III burst. Only those channels with a modulation factor exceeding .20 were used.

The direction-finding results yield only the direction of arrival. To compute the heliocentric radial distance of the type III burst it is necessary to use a model of the solar wind density. For the events analyzed the RAE emission level scale, assuming second harmonic emission, was used. Where it was possible the emission level

scale was adjusted so that the density at 1.0 AU agreed with in situ measurements. An Archimedean spiral is fit through the source locations projected into the ecliptic plane. A solar wind velocity of 400 km sec^{-1} was used to construct the Archimedean spiral. Since HAWKEYE 1's spin plane is not oriented exactly perpendicular to the ecliptic plane it is necessary to know the φ_{GSE} coordinate of the source position before λ_{GSE} can be determined. If φ_{GSE} could not be determined from the IMP 8 data it was computed from the least squares fit Archimedean spiral through the available IMP 8 data points. Errors in λ_{GSE} caused by computing φ_{GSE} are estimated to be smaller than 3°. The GSE latitudes (λ_{GSE}) and GSE longitudes (φ_{GSE}) for the three events are summarized in Table I. Any λ_{GSE} in Table I that required the Archimedean spiral fit to compute φ_{GSE} is indicated by an asterisk.

A. Direction of Arrival Analysis

1. June 8, 1974 1400-1600 UT

For the first event analyzed, shown in Figure 12, the RAE emission level (assuming second harmonic emission) was adjusted to agree with the local plasma density. The levels were adjusted so that emission at 1.0 AU would occur at 44 kHz. The emission levels give the heliocentric radial distance at which the burst occurs for the various frequencies. Plasma oscillations (probably not due to solar electrons) were observed in the 22 kHz channel on IMP 8, thus type III emission at 1.0 AU would probably occur at 44 kHz. An

Archimedean spiral was least squares fit to the 500 kHz, 178 kHz, 100 kHz and 56.2 kHz IMP 8 data. The spiral, representing the magnetic field line along which the electrons generating the type III burst travel, is near the earth; therefore, the local plasma density at the earth is probably close to the plasma density at 1.0 AU along this trajectory. The upper left-hand panel in Figure 12 shows the source locations projected into the ecliptic plane and the least squares fit Archimedean spiral through the source locations. The lower left-hand panel shows the Geocentric Solar Ecliptic longitude (φ_{GSE}) of the least squares fit Archimedean spiral as viewed from earth as a function of heliocentric radial distance. The experimental values of φ_{GSE} are also shown.

Since φ_{GSE} is not available from direct measurements by IMP 8, at 42.2 kHz and 31.1 kHz, φ_{GSE} was calculated from the least squares fit Archimedean spiral for these two frequencies. These calculated longitudes are used with the HAWKEYE 1 data to determine the latitude at 42.2 kHz and 31.1 kHz. The upper right-hand panel in Figure 12 shows the heliocentric latitude of the source location as a function of frequency, and the least squares fit magnetic field line using the constant latitude model. The heliocentric coordinate system has its X axis along the sun-earth line and its Z axis perpendicular to the ecliptic plane. The lower right-hand panel shows the Geocentric Solar Ecliptic latitudes (λ_{GSE}) of the best fit field line as a function of heliocentric radial distance and the observed λ_{GSE} of the source locations.

For this event the ehliocentric latitude of the source locations fit poorly to the constant latitude model of the solar magnetic field. At 42.2 kHz and 31.1 kHz the heliocentric radial distance is greater than 1.0 AU, thus the radiation must propagate towards the sun to be observed by the spacecraft. As the frequency of the emission approaches the plasma frequency, scattering and refraction become important. The modulation factor of the 31.1 kHz HAWKEYE 1 channel is very low, making it difficult to obtain accurate measurements of the source location at this frequency. The measurements taken with the 56.2 and 42.2 HAWKEYE 1 channels indicate that the source locations lie near the ecliptic plane suggesting that for this event the magnetic field may be best represented by the convergent field line model (Figure 11).

The most probable flare location is found by extrapolating the magnetic field line obtained from the constant latitude model back to the sun. The actual flare location differs from the most probable flare location by one degree in heliocentric latitude and twelve degrees in heliocentric longitude.

2. July 5, 1974 2130-2300 UT

The RAE emission level scale was not adjusted for this event because the trajectory of the burst was so far from the earth that the densities measured by IMP 8 could not be considered representative of the density at 1.0 AU along the trajectories of the burst. From July 4 to July 9 the density varied considerably, indicating that the density at the earth may have been significantly different than the density at the source location. The emission level used in

this analysis predicts a second harmonic emission at 57 kHz for a radial distance of 1.0 AU. The 500 kHz and 56.2 kHz IMP 8 channels were contaminated with non-type III radiation and thus were not used in the analysis. An Archimedean spiral was fit to the IMP 8 178 kHz and 100 kHz channels. The longitudinal positions necessary for the determination of λ_{GSE} for the 56.2 kHz and 42.2 kHz channels were calculated from the least squares fit Archimedean spiral through the 178 kHz and 100 kHz IMP 8 channels. The upper left-hand panel in Figure 13 shows the source locations projected into the ecliptic plane and the least squares fit Archimedean spiral through the source locations. The lower left-hand panel shows the Geocentric Solar Ecliptic longitude of the least squares fit Archimedean spiral and the experimental values of φ_{GSE}. The upper right-hand panel shows the heliocentric latitude of the source locations and the least squares fit magnetic field line using the constant latitude model. The lower right-hand panel shows the Geocentric Solar Ecliptic latitudes of the source locations and the least squares fit magnetic field line.

The latitude of the 100 kHz emission is smaller than what would be predicted by the constant latitude model. If the 100 kHz channel is not used the best fit heliocentric latitude for the magnetic field line is 31°S. A heliocentric latitude of 31°S is consistent with the constant latitude model. With the 100 kHz channel used in the analysis the best fit heliocentric latitude is 25°S. The accuracy of the latitude for the 42.2 kHz emission is probably reduced because of scattering and retraction of the radiation. The flare

location associated with this event is 16°S 26°W [NOAA, 1975]. The extrapolation of the best fit magnetic field line (with the 100 kHz channel used in the analysis) to the sun predicts a flare location of 25°S 32°W.

3. July 6, 1974 1030-1300 UT

For this event, shown in Figure 14, the emission level scale was also not adjusted due to the density changes that occurred between July 4 and July 9 and the large distance from the earth of the source locations. An Archimedean spiral is least squares fit to the longitudes of the 500 kHz, 178 kHz and 100 kHz IMP 8 channels. The longitudinal source locations were calculated from the least squares fit Archimedean spiral for the 56.2 kHz, 42.2 kHz and 31.1 kHz channels. The calculated φ_{GSE} is used for the calculation of λ_{GSE} for the HAWKEYE 1 56.2 kHz, 42.2 kHz, and 31.1 kHz channels. The left-hand panels in Figure 14 show the measured longitude and least squares fit longitude of this burst. The right-hand panels show the measured latitudes and least squares fit latitude of this burst.

This event is best represented by the constant latitude model for all the frequencies. The extrapolation of the least squares field line back to the sun predicts a flare location of 17°S 39°W compared to the probable flare location of 17°S 30°W, [NOAA, 1974].

B. Source Size of Type III Bursts

The modulation factor of the emissions can give an estimate of the source size when the elevation angle, α, of the source is known.

The source size is defined as the angle between a line from the observer to the centroid of the source and a line from the observer to the edge of the source. Figures 15 and 16 give the modulation factor as a function of half angle source sizes as observed from the satellite for various elevations for two source models. α is the elevation angle. The first model, shown in Figure 15, is for a source which is modeled as a thin, flat disk with the intensity of radiation emitted from the disk uniformly distributed. For a given source size the solid angle of the disk remains constant for all elevation angles. The modulation factor for the disk model decreases with increasing source size until the modulation factor is zero. (The source size at which the modulation factor goes to zero is less than 90°.) Then the source size increases in angle, the null angle shifts by 90° and the modulation then increases with increasing source size. The disk model breaks down for large elevations with large source sizes.

The second model of the source assumes that the source region is a sphere where the intensity of radiation emitted from each volume element is uniform. Figure 16 gives the modulation as a function of source size as viewed from the earth and elevation angle for a spherical source. The spherical source model has the complication that if the source is large, the satellite will probably be inside the source region, but does not have the problem that the modulation increases with increasing source size for very large sources. If the satellite is inside the source, the size of the source may be computed because the modulation factor is a function of the ratio of the radial distance, R, from the center of the source to the earth (or

satellite) and the radius of the source, R_S. The center of the source can be found from the RAE emission level scale and the direction finding measurements. Once the position of the center of the source is known, the radial distance R from the center of the source to the earth can easily be computed. The modulation factor gives us R/R_S, hence $R_S = (\frac{1}{R/R_S}) \times R$. The half angle source size as viewed from the sun can then be computed from R_S and the position of the center of the source. The computed source sizes represent the longitudinal extent of the source. Figure 17 shows the source size of the first event analyzed as viewed from the earth for a disk source. As would be expected, the source size increases with decreasing frequency (or increasing radial distance from the sun). Figure 18 shows the source sizes for a disk source as viewed from the sun for the same event. The modulation factor, m, for 500 kHz is .855, for 178 kHz m = .691, for 100 kHz m = .467, and for 56.2 kHz m = .230. The source sizes are on the average over twice as large as the 60° full width half maximum values that Lin [1974] and Alvarez et al. [1975] observe for the particle fluxes in a type III event, but source size does remain relatively constant over the range of radial distances. Scattering of the radio emissions may be responsible for the large apparent source sizes. If the source is assumed as spherical, the satellite is inside the source at 100 kHz and 56.2 kHz, but the source sizes viewed from the sun do not differ significantly from the disk source model.

VII. DISCUSSION

Two of the three type III events presented in this paper are in agreement with the constant latitude model of the solar magnetic field. One event (June 8) is more consistent with the convergent field line model. For this event the magnetic field lines at radial distances from the sun of less than 1.0 AU appears to move to lower heliocentric latitudes with increasing radial distance as in the convergent field line model. At a radial distance greater than 1.0 AU the latitude is consistent with the constant field line model, but the error involved in the measurement at 31.1 kHz is quite large due to the lower modulation at this frequency. However the convergent field line model contradicts some measurements of the skewing of the magnetic field away from the equatorial plane which have been made at 1.0 AU [Coleman and Rosenberg, 1971; Rosenberg and Wing, 1974]. None of the data anlyzed indicates that the magnetic field lines cross the ecliptic plane or that the divergent field line model is valid. Additional evidence supporting the constant latitude model is that the predicted flare locations are in good agreement with the observed flare locations.

The data presented is consistent with the assumption of emission at the second harmonic for the frequencies analyzed. The fact that type III emissions are seen at low frequencies for flare locations

with large range of longitude (fundamental radiation would have a much narrower cone of emission), and the fact that large differences in densities are rarely seen [Hundhausen, 1968] indicates that the observed radiation is primarily at the second harmonic of the plasma frequency.

However there are some features of type III bursts that might be explained by radiation at both the fundamental and second harmonic. The source sizes measured are a factor of two larger than the angular sizes of the solar electron emissions from a flare reported by Lin [1974] and Alvarez et al. [1975]. The modulation factor tends to be largest near the beginning of an event, and the direction of arrival of the radiation varies systemmatically during the event, usually starting near the sun and deviating away from the sun later in the event.

If a type III burst radiates at both the fundamental and second harmonic of the plasma frequency signals would be received from two source locations. One source location would correspond to the fundamental emission region and the other source location would correspond to the second harmonic emission region. With two separate sources of electromagnetic radiation the modulation factor decreases very rapidly as the angular separation between the two sources increases. The modulation factor of a signal received from two separate sources will be much lower than the modulation factor of the signal received from a single source model (thin, flat disk source model or spherical source model) with the angular source size of the single source equal

to the angular separation of the two separate sources. With simultaneous emission of both fundamental and second harmonic radiation the received signal would be from two separate source regions and the modulation factor would be much lower than the modulation factor for a single source, making the source size appear to be very large. This may explain why the observed source sizes are larger than the source sizes determined from particle flux measurements.

If a stream of particles generating a type III burst moves outward from the sun and generates emission at both the fundamental and second harmonic of the plasma frequency the radiation near the start of the burst would be predominantly fundamental emission and near the end of the burst the radiation would be predominantly second harmonic. The apparent source size of the fundamental emission would be smaller than the apparent source size of the second harmonic emission for several reasons. Since the size of the emission region increases with increasing heliocetric radial distance, the fundamental emission region would be smaller because it is generated closer to the sun. The source region for the fundamental emission is usually farther from the earth than the second harmonic source region; thus, the apparent source size would be smaller for the fundamental emission. Therefore, the modulation factor would be larger near the start of the event as is observed.

The shift in the direction of arrival of the radiation could be explained by emission containing both fundamental and second harmonic radiation. The fundamental emission region would be closer to the sun

than the second harmonic emission region; therefore, for most Archimedean spiral positions the direction of the source would start near the sun and drift away from the sun in a systemmatic way, as is observed in many cases. An example of the shift in direction of arrival at 100 kHz is shown in Figure 8. Initially φ_{GSE} is near zero, possibly caused by emission predominantly at the fundamental, then near the end of the event φ_{GSE} is approximately 45°, possibly caused by emission predominantly at the second harmonic. For events which have a large enough modulation factor in the 56.2 kHz channel a similar effect is seen. φ_{GSE} will also be near zero, but will shift to a larger angle than what is seen for the 100 kHz channels. The larger angular shift during the type III event for the lower frequencies is consistent with emission at the fundamental and second harmonic since the angular separation between the fundamental source location and the second harmonic source location is greater at the lower frequencies.

There are other possible explanations for the systemmatic drifts in source location and variations in the modulation factor which should also be considered. Irregularities in the solar wind density could cause different regions to radiate at the same frequency at different times thus causing the observed changes in the angular position of the source. If there are several regions of the source that are more intense than the rest of the source the most intense region would dominate in the direction-finding analysis. As different regions change in intensity the source location will appear to change. The changes in source location would be expected to be random unless

there were some systematic longitudinal variation in the electron flux or solar wind density while the burst is being generated. The source sizes are large enough that the changes in the source location could be as large as the observed angle drifts. The angular separation of these regions as viewed from the earth would be larger for the lower frequencies, thus the angle drifts would be expected to be larger for the lower frequencies. As more regions begin to radiate as the burst progresses the source size will grow and the modulation factor would decrease as a function of time.

If the radiation is not circular or randomly polarized, changes in the polarization could affect the direction-finding measurements and produce a shift in the source location. The effects due to polarization increase as the angle α (the angle between the plane of rotation of the antenna and the source location) increases. α is generally larger for the lower frequencies thus polarization effects, i.e., a shift in the source location, would be greater for the lower frequencies as is the case for the data presented in this paper. At high frequencies the type III radiation has circular or random polarization if viewed by receivers with a wide bandwidth. The IMP 8 and HAWKEYE 1 receivers have a wide bandwidth.

Although irregularities in the solar wind density or polarization effects may cause the systematic drift in the direction of arrival of radiation from a type III event at one frequency, there is currently no completely adequate explanation of the drift in source position. Although the changes in the direction of arrival could be

caused by a combination of fundamental and second harmonic emission there is still no direct evidence that emission occurs at both frequencies. Fainberg and Stone [1974] presents the review of the results from many thousands of events with no evidence that the emission occurs at both the fundamental and second harmonic at low frequencies. Even if the emission did occur at both the fundamental and second harmonic, the fundamental would probably not always be observed since the cone of emission for the fundamental radiation is much smaller than the cone of emission for radiation at the second harmonic. (It cannot be assumed that the fundamental emission occurs along a density enhancement, as a density enhancement is rarely seen [Hundhausen, 1968].) It would also be extremely difficult to separate the fundamental and second harmonic emissions from each other since both emissions would be occurring nearly simultaneously.

The effects of changes in the source position are thought to be reduced in this study since the source locations are averaged over the duration of the event. However, the explanation of the drift may provide important insight into the type III emission processes in the solar wind and should be studied in detail.

The results of the analysis presented in this paper are model dependent. It is necessary to use a density scale to determine the heliocentric radial distance at which the radiation is generated. The requirement to assume a density model can be eliminated if the source position is determined by triangulation. For example, simultaneous direction-finding measurements from three spacecraft, two

located near the earth to establish the earth-source line and one located far from the earth to determine the source position along the line, can provide measurements of this type. We hope that simultaneous radio direction-finding measurements from the HELIOS 1 and 2 spacecraft, which are now in orbit around the sun, and from the IMP 8 and HAWKEYE 1 satellites near the earth will be able to provide such measurements. If successful, these multi-spacecraft direction-finding measurements will make it possible to study the three-dimensional structure of the magnetic field in the solar wind completely independent of any modeling assumptions.

LIST OF REFERENCES

Alexander, J. K., H. H. Malitson, and R. G. Stone, Type III radio bursts in the outer corona, Solar Phys., 8, 388-397, 1969.

Alvarez, H. and F. T. Haddock, Solar wind density model from KM-wave type III bursts, Solar Phys., 29, 197-209, 1973.

Alvarez, H., F. T. Haddock, and R. P. Lin, Evidence for electron excitation of type III radio burst emission, Solar Phys., 26, 468-473, 1972.

Alvarez, H., R. P. Lin, and S. J. Bame, Fast solar electrons, interplanetary plasma and KM-wave type III radio bursts observed from the IMP-6 spacecraft, Solar Phys., 44, 485-501, 1975.

Coleman, P. J., Jr. and R. L. Rosenberg, The north-south component of the interplanetary magnetic field, J. Geophys. Res., 76, 2917-2926, 1971.

Fainberg, J., L. G. Evans, and R. G. Stone, Radio tracking of solar energetic particles through interplanetary space, Science, 178, 743-745, 1972.

Fainberg, J. and R. G. Stone, Type III solar radio burst storms observed at low frequencies (Part I Storm Morphology), Solar Phys., 15, 222-233, 1970a.

Fainberg, J. and R. G. Stone, Type III solar radio burst storms observed at low frequencies (Part II Average Exciter Speed), Solar Phys., 15, 433-445, 1970b.

Fainberg, J. and R. G. Stone, Type III solar radio burst storms observed at low frequencies (Part III Streamer Density, Inhomogeneities and solar wind speed), Solar Phys., 17, 392-401, 1971.

Fainberg, J. and R. G. Stone, Satellite observations of type III solar radio bursts at low frequencies, Space Sci. Rev., 16, 145-188, 1974.

Frank, L. A. and D. A. Gurnett, Direct observations of low-energy solar electrons associated with a type III solar radio burst, Solar Phys., 27, 446-465, 1972.

Ginzburg, V. L. and V. V. Zhelezniakov, On the possible machanisms of sporadic solar radio emission (radiation in an isotropic plasma), Sov. Astron., AJ2, 653-668, 1958.

Gurnett, D. A. and L. A. Frank, Electron plasma oscillations associated with type III radio emissions and solar electrons, accepted for publication, Solar Phys., 1975.

Haddock, F. T. and H. Alvarez, The prevalence of second harmonic radiation in type III bursts observed at kilometric wavelengths, Solar Phys., 29, 183-196, 1973.

Haddock, F. T. and T. E. Graedel, Dynamic spectra of type III solar bursts from 4 to 2 MHz observed by OGO-III, Astrophys. J., 160, 293-300, 1970.

Hartz, T. R., Solar noise observations from the Alouette satellite, Ann. Astrophys., 27, 831-836, 1964.

Hartz, T. R., Type III solar radio noise bursts at hectometer wavelengths, Planet. Space Sci., 17, 267-287, 1969.

Hundhausen, A. J., Direct observations of solar wind particles, Space Sci. Rev., 8, 690-749, 1968.

Kaiser, M. L., The solar elongation distribution of low frequency radio bursts, Solar Phys., 45, 181-187, 1975.

Kellogg, P. J., J. C. Lai, and D. G. Cartwright, Kilometric wave observations of the great type III burst of August 7, 1972, World Data Center A Report UAG-28, Part II, 288-290, 1973.

Kundu, M. R., Solar Radio Astronomy, Interscience, New York, 1965.

Lin, R. P., The emission and propagation of ~ 40 keV solar flare electrons, Solar Phys., 12, 266-303, 1970.

Lin, R. P., Non-relativistic solar electrons, Space Sci. Rev., 16, 189-256, 1974.

Lin, R. P., L. G. Evans, and J. Fainberg, Simultaneous observations of fast solar electrons and type III radio burst emission near 1 AU, Astrophys. Letters, 14, 191-198, 1973.

Newkirk, G., Jr., Structure of the solar corona, Ann. Rev. Astron. Astrophys., 5, 213-266, 1967.

NOAA Solar-Geophysical Data, No. 364, Part II, December 1974.

NOAA Solar-Geophysical Data, No. 365, Part II, January 1975.

Parker, E. N., Interplanetary Dynamical Processes, Interscience, New York, 1963.

Parker, E. N., The penetration of galactic cosmic rays into the solar system, The Solar Wind, Pergamon Press, Oxford, 1964.

Parker, E. N., Dynamical theory of the solar wind, Space Sci. Rev., 4, 666-708, 1965.

Rosenberg, R. L. and C. R. Winge, Jr., The latitude dependencies of the solar wind, Solar Wind Three, Institute of Geophysics and Planetary Physics, UCIA, 300-310, 1974.

Schatten, K. H., Large-scale properties of the interplanetary magnetic field, Solar Wind, NASA publication #SP-308, 65-92, 1972.

Schatten, K. H., N. F. Ness, and J. M. Wilcox, Influence of a solar active region on the interplanetary magnetic field, Solar Physics, 5, 240-256, 1968.

Slysh, V. I., Long-wavelength solar radio emissions observed by the lunar satellites Luna 11 and Luna 12, Cosmic Research, English transl., 5, 759-769, 1967.

Smith, D. F., Type III solar radio bursts, Adv. Astron. Astrophys., 7, 147-226, 1970.

Smith, D. F., Type III radio bursts and their interpretation, Space Sci. Rev., 16, 91-144, 1974.

Stone, R. G., Traveling solar radio bursts, Solar Wind Three, Institute of Geophysics and Planetary Physics, UCLA, 72-97, 1974.

Suess, S. T., Three dimensional modelling, Solar Wind Three, Institute of Geophysics and Planetary Physics, UCLA, 311-317, 1974.

Suess, S. T., A. J. Hundhausen, and V. Pizzo, Latitutde dependent non-linear high-speed solar wind streams, J. Geophys. Res., 80, 2023-2029, 1975.

Suess, S. T. and S. F. Nerney, The global solar wind and predictions for Pioneers 10 and 11, Geophys. Res. Lett., 2, 75-77, 1975.

Van Allen, J. A. and S. M. Krimigis, Impulsive emission of ~ 40-keV electrons from the sun, J. Geophys. Res., 70, 5737-5751, 1965.

Wilcox, J. M. and N. F. Ness, Solar source of the interplanetary sector structure, Solar Phys., 1, 437-445, 1967.

Wild, J. P., Observations of the spectrum of high-intensity solar radiation at metre wavelengths (III Isolated bursts), Aust. J. Sci. Res., A3, 541-557, 1950.

Wild, J. P. and L. L. McCready, Observations of the spectrum of high-intensity solar radiation at metre wavelengths (I. The apparatus and spectral types of solar bursts observed), Aust. J. Sci. Res., A3, 387-398, 1950.

Wild, J. P., J. D. Murray, and W. C. Rowe, Harmonics in the spectra of solar radio disturbances, Aust. J. Phys., 7, 439-459, 1954.

Wild, J. P., K. V. Sheridan, and A. A. Neylan, An investigation of the speed of the solar disturbances responsible for type III radio bursts, Aust. J. Phys., 12, 369-398, 1959.

APPENDIX 1: TABLES

TABLE 1

LATITUDE AND LONGITUDE OF TYPE III RADIO BURSTS
(GEOCENTRIC SOLAR ECLIPTIC COORDINATES)

June 8, 1974

Frequency	Latitude	Longitude
500 kHz	--	$-7° \pm 1°$
178 kHz	--	$-16° \pm 1°$
100 kHz	$-24° \pm 6°$	$-20° \pm 1°$
56.2 kHz	$-11° \pm 7°$	$9° \pm 1°$
42.2 kHz	$-10° \pm 9°$ *	--
31.1 kHz	$-32° \pm 32°$ *	--

July 5, 1974

Frequency	Latitutde	Longitude
178 kHz	$-21° \pm 7°$	$-2° \pm 1°$
100 kHz	$-20° \pm 2°$	$15° \pm 6°$
56.2 kHz	$-30° \pm 16°$ *	--
42.2 kHz	$-32° \pm 25°$ *	--

July 6, 1974

Frequency	Latitutde	Longitude
500 kHz	--	$-5° \pm 1°$
178 kHz	--	$-8° \pm 1°$
100 kHz	--	$4° \pm 1°$
56.2 kHz	$-31° +8°$ *	--
42.2 kHz	$-25° +15°$ *	--
31.1 kHz	$-11° \pm 15°$ *	--

* Involves model fitting, not a direct measurement.

APPENDIX 2: FIGURES

Figure 1. The IMP 8 orbit projected into the ecliptic plane. The angle δ_y is the angle from the projection of the satellite-sun line into the spin plane to the antenna. The angle δ_y at which a null of the modulated signal occurs determines a meridional plane through the spin axis in which the source must be located. The approximate location of the HAWKEYE 1 orbit plane is also indicated.

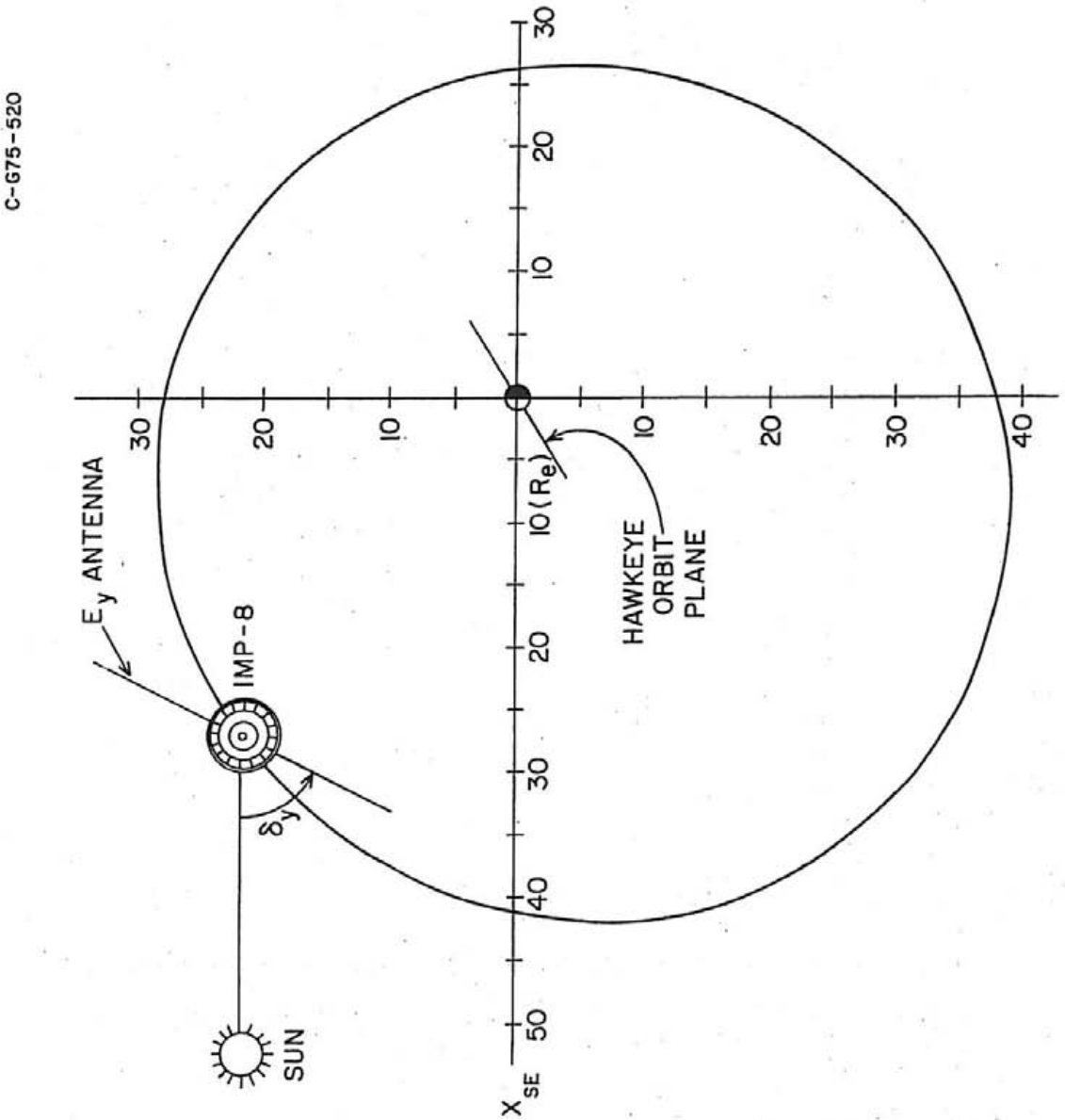
C-G75-520
30
20
10
10
20
30
40
Y_{SE}
$10(R_E)$
HAWKEYE
ORBIT
PLANE
E_y ANTENNA
IMP-8
δ_y
SUN
X_{SE}
50
40
30
20
10

Figure 1

Figure 2 The HAWKEYE 1 orbit plane and spin axis orientation relative to the orbit plane. The angle δ_y is the angle from the projection of the satellite-sun line into the spin plane to the antenna. The angle δ_y at which a null of the modulated signal occurs determines a meridional plane through the spin axis in which the source must be located. The IMP 8 spin axis orientation and orbit plane are shown relative to the HAWKEYE 1 orbit.

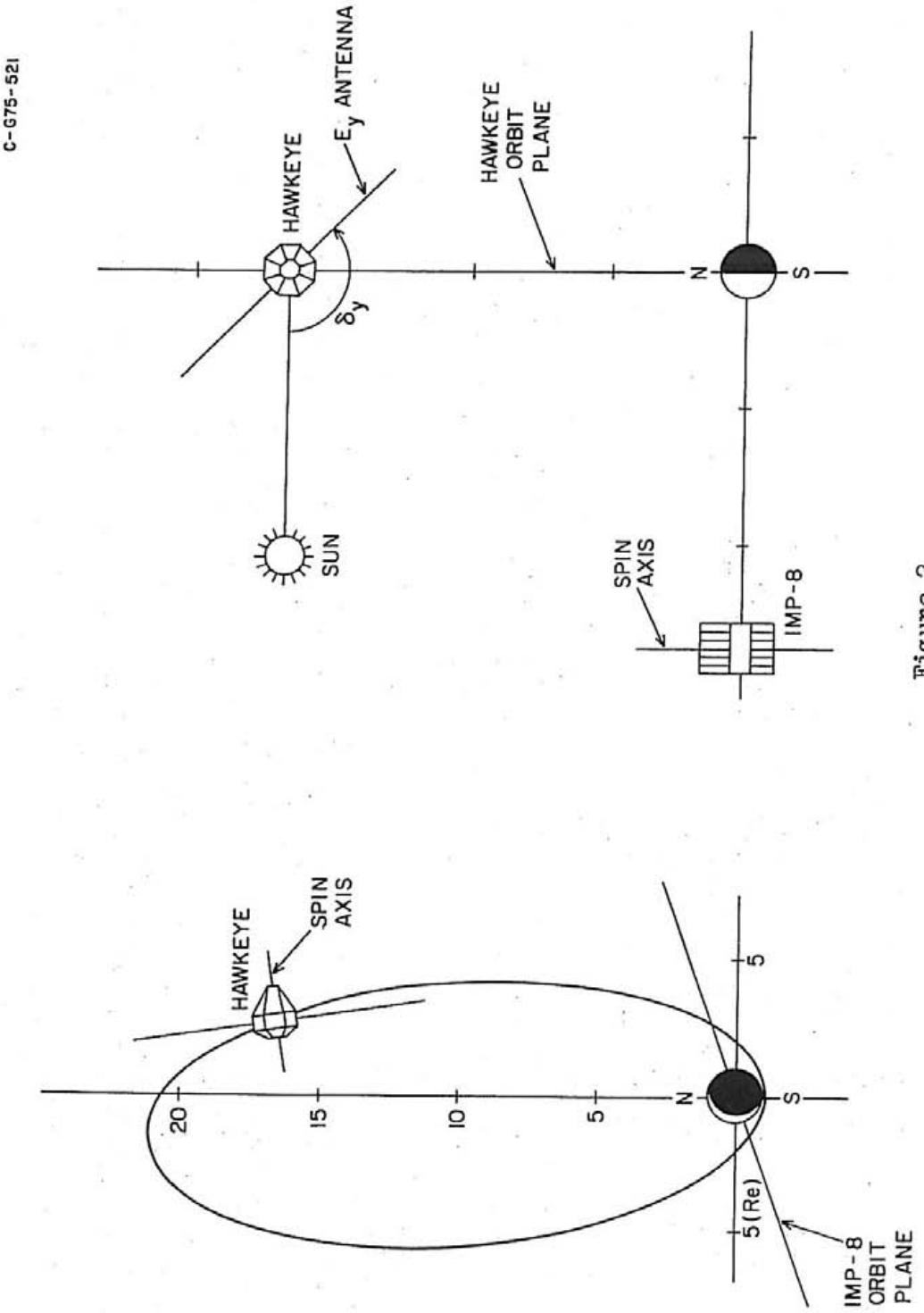
C-675-521
HAWKEYE
E_y ANTENNA
HAWKEYE ORBIT PLANE
δ_y
SUN
SPIN AXIS
IMP-8
N
S
HAWKEYE
SPIN AXIS
20
15
10
5
5
5(Re)
IMP-8 ORBIT PLANE

Figure 2

Figure 3 The normalized electric field amplitude as a function of the antenna orientation angle δ_y for a type III burst at 178 kHz. The modulation pattern is clearly observed. δ is the position of the null computed by a least squares fit of the data to the theoretical modulation pattern. Each point is the average of many data points accumulated in the 10° angle bins.

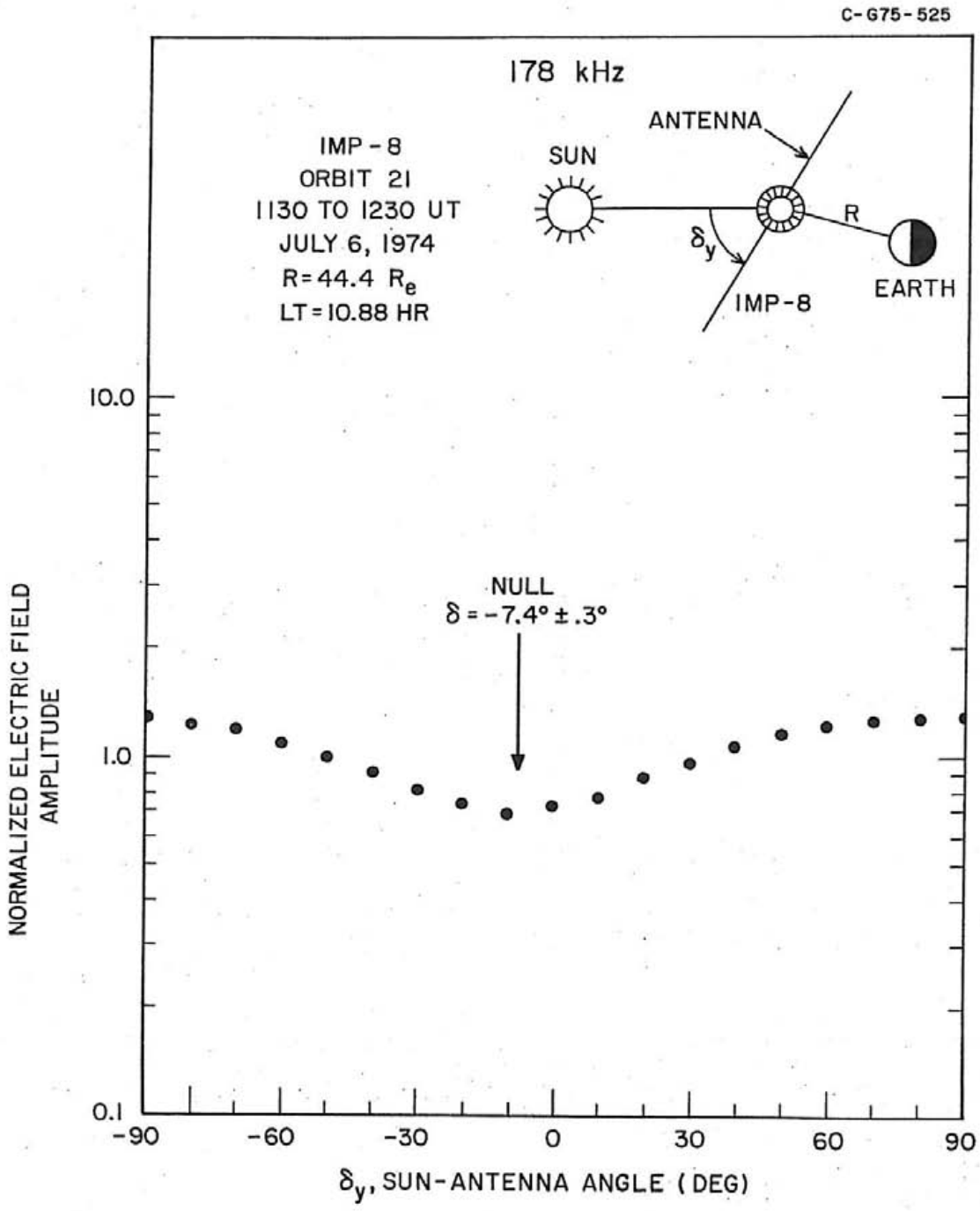
C-G75-525
178 kHz
IMP-8
ORBIT 21
1130 TO 1230 UT
JULY 6, 1974
R=44.4 Re
LT=10.88 HR
SUN
ANTENNA
R
δy
IMP-8
EARTH
NULL
δ = -7.4° ± .3°
NORMALIZED ELECTRIC FIELD AMPLITUDE
10.0
1.0
0.1
-90
-60
-30
0
30
60
90
δy, SUN-ANTENNA ANGLE (DEG)

Figure 3

Figure 4 The position of the source plane relative to the satellite spin axis, null position (δ), and the sun for HAWKEYE 1 and IMP 8. The vector $\hat{n}$ is perpendicular to the source plane, and the spin axis ($\vec{S}$) is perpendicular to the spin plane. The source planes for IMP 8 and HAWKEYE 1 intersect, and the source is located along this intersection. The source location is computed by taking the cross product between $\hat{n}_1$, a vector normal to the IMP-8 source plane, and $\hat{n}_2$, a vector normal to the HAWKEYE 1 source plane. θ is the angle between the spin axis of the satellite and the satellite-sun line.

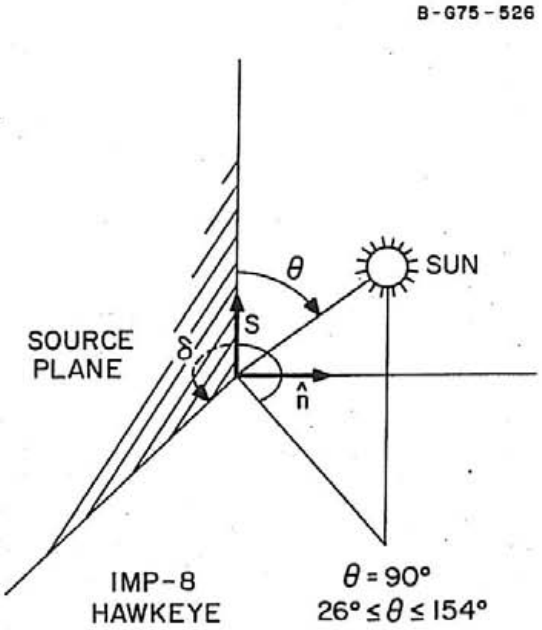
B-G75-526
θ
SUN
S
SOURCE
PLANE
δ
n̂
IMP-8
HAWKEYE
θ = 90°
26° ≤ θ ≤ 154°

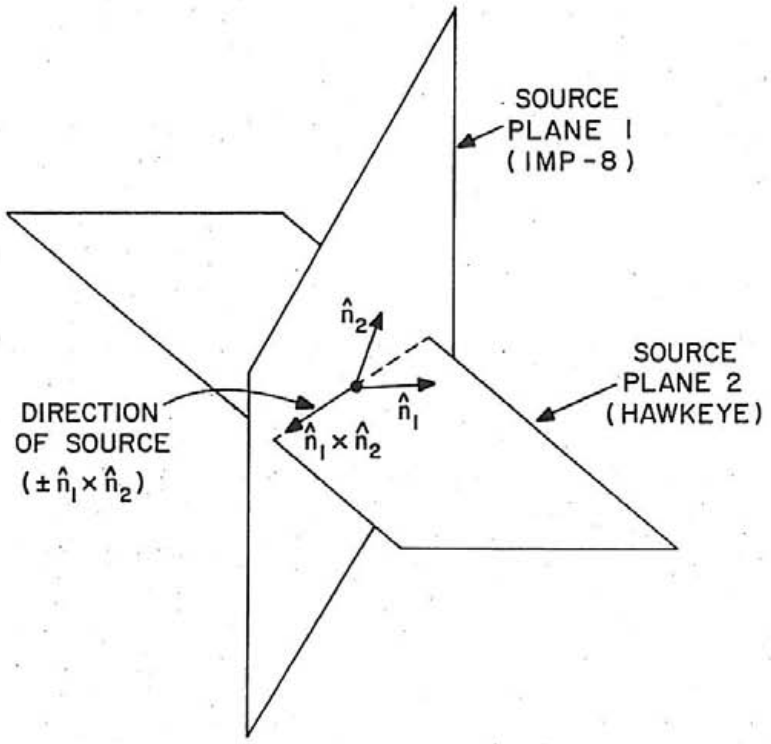
SOURCE
PLANE 1
(IMP-8)
n̂2
SOURCE
PLANE 2
(HAWKEYE)
n̂1
DIRECTION
OF SOURCE
(± n̂1 × n̂2)
n̂1 × n̂2

Figure 4

Figure 5 A type III burst observed simultaneously by HAWKEYE 1 and IMP 8. The type III burst is characterized by a rapid decrease in frequency with increasing time, and at each frequency the intensity has a rapid rise time followed by a slower exponential decay.

C-G75-781-I

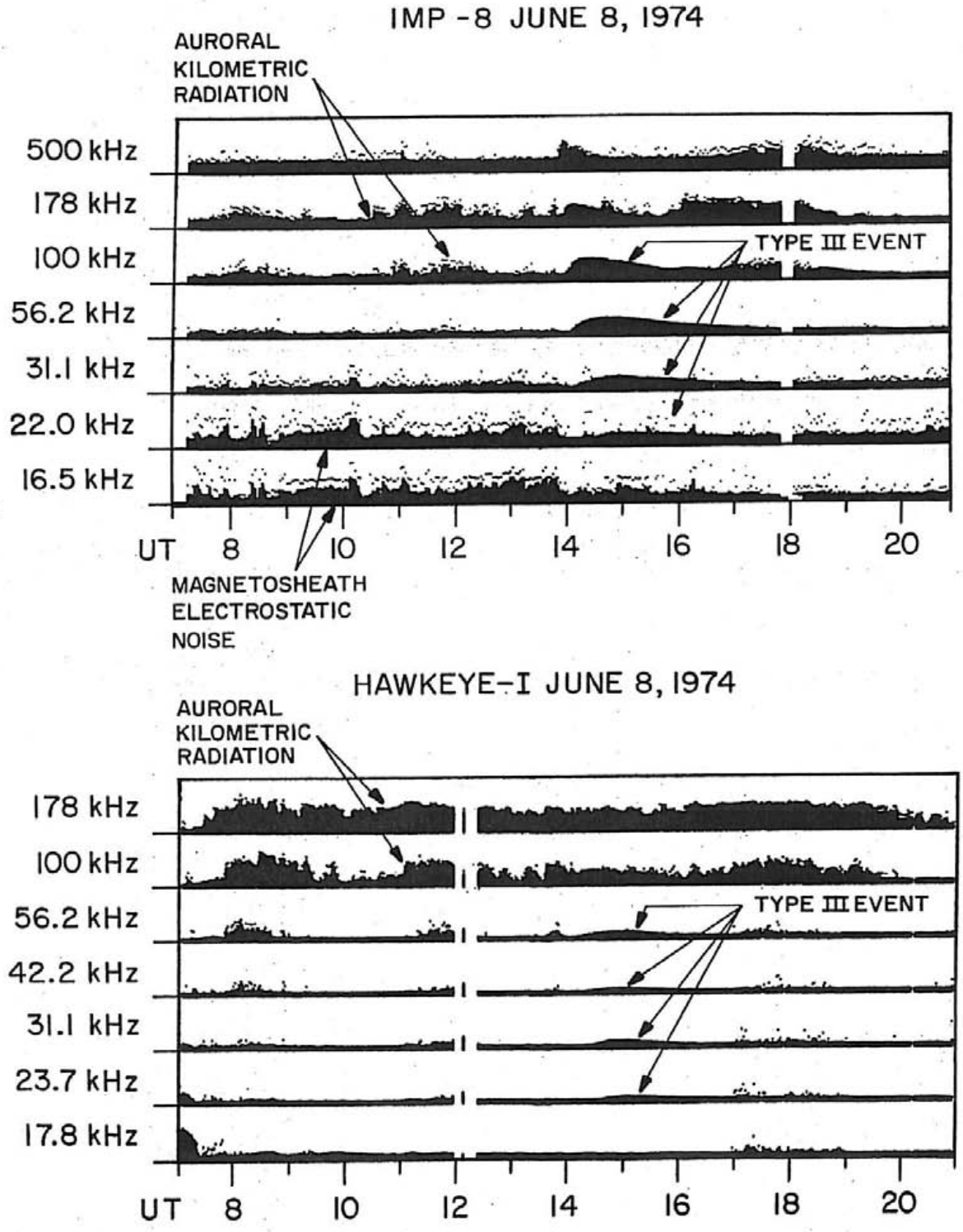

Figure 5

Figure 6 The amplitude, Geocentric Solar Ecliptic longitude and modulation factor of a type III burst detected by IMP 8 on June 10 at 500 kHz. Note the strong modulation and that φ_{GSE} is relatively constant at this frequency. The spin modulation is evident as a small amplitude, periodic change in the observed intensity. The angular position of the earth is shown to help discriminate between solar and terrestrial events.

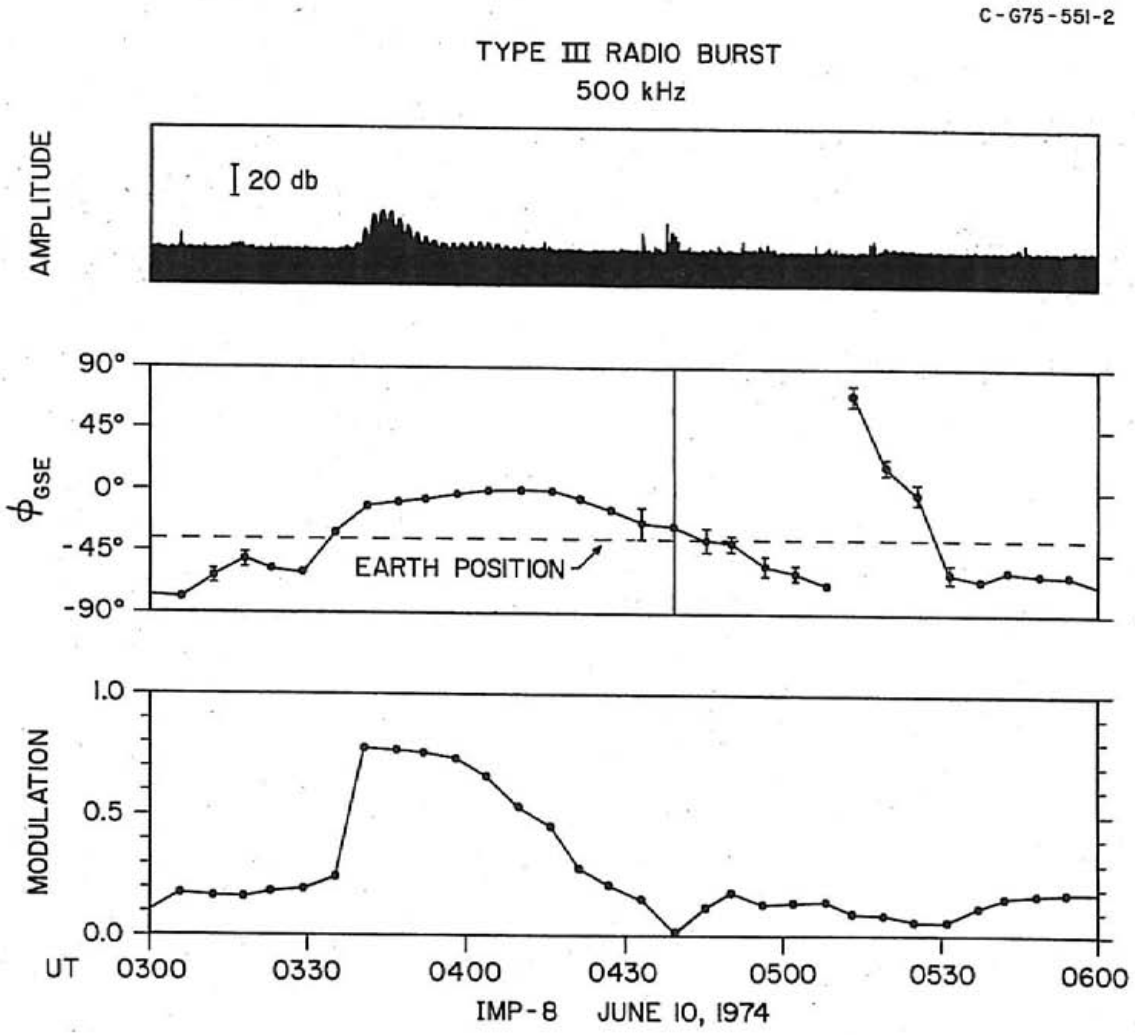
C-G75-551-2
TYPE III RADIO BURST
500 kHz
AMPLITUDE
20 db
90°
45°
0°
-45°
-90°
ϕ_{GSE}
EARTH POSITION
1.0
0.5
0.0
MODULATION
UT
0300
0330
0400
0430
0500
0530
0600
IMP-8 JUNE 10, 1974

Figure 6

Figure 7 The amplitude, Geocentric Solar Ecliptic longitude and modulation factor for a type III event detected by IMP 8 on June 9 at 178 kHz. Note the modulation factor is lower and that φ_{GSE} changes during the event. There is a terrestrial noise source with a large modulation factor being detected before and after the type III event.

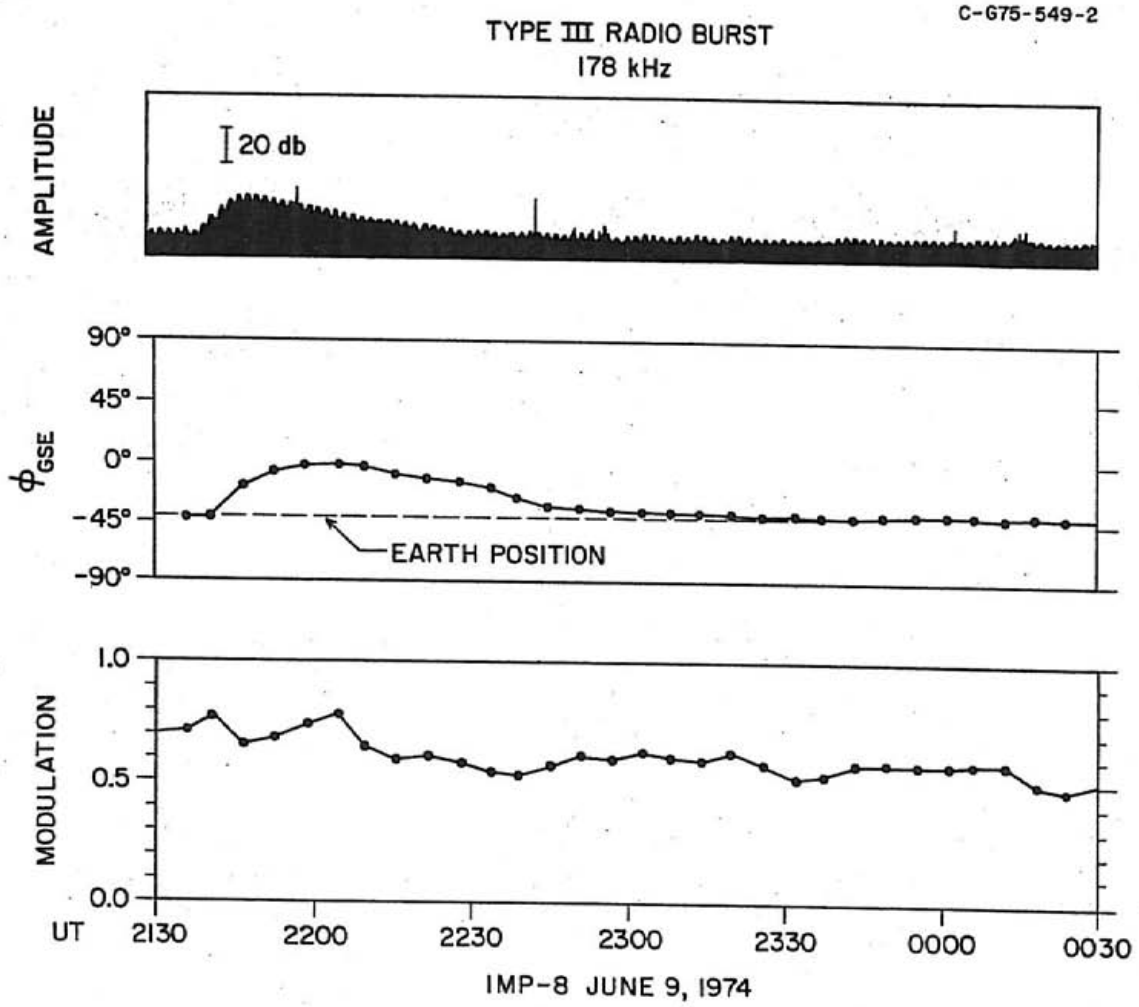
C-G75-549-2
TYPE III RADIO BURST
178 kHz
AMPLITUDE
20 db
90°
45°
0°
-45°
-90°
ϕ_{GSE}
EARTH POSITION
1.0
0.5
0.0
MODULATION
UT
2130
2200
2230
2300
2330
0000
0030
IMP-8 JUNE 9, 1974

Figure 7

Figure 8 The amplitude, Geocentric Solar Ecliptic longitude, and modulation factor for a type III event detected by IMP 8 on June 21 at 100 kHz. The duration of this event is considerably longer than the duration of events at 500 kHz and 178 kHz. The longitude of the source location also changes over a greater range than at 500 kHz or 178 kHz. The longitude drifts from near zero degrees near the beginning of the event to about 45° near the end. The modulation factor near the beginning of the event averages about 0.65, dropping to about 0.25 at the end of the event. The apparent shift in source location could be caused by polarization effects, density inhomogeneities, or by radiation from different source regions at both the fundamental and second harmonic of the plasma frequency.

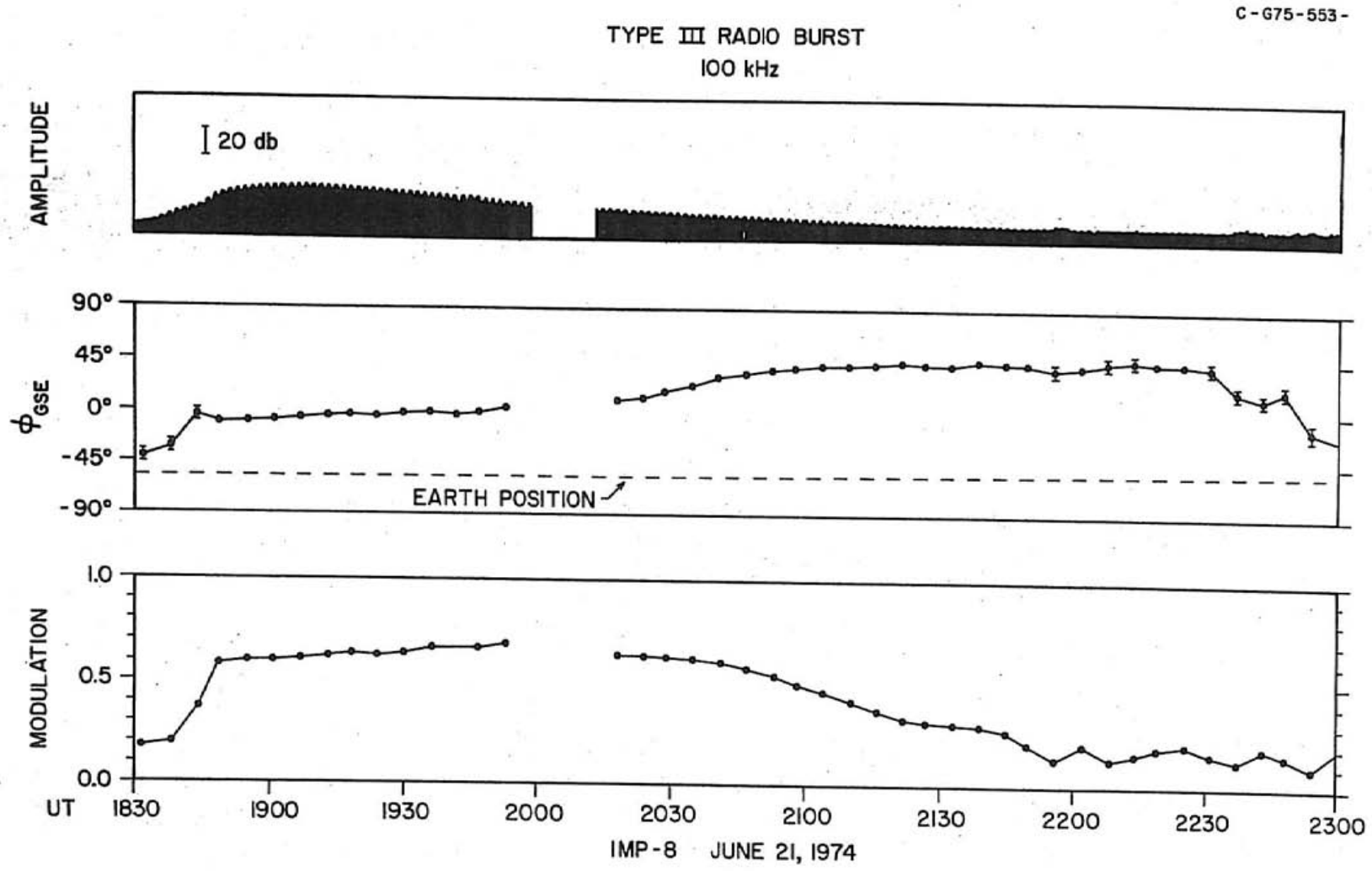
C-G75-553-
TYPE III RADIO BURST
100 kHz
AMPLITUDE
20 db
90°
45°
0°
-45°
-90°
ϕ_{GSE}
EARTH POSITION
1.0
0.5
0.0
MODULATION
UT
1830
1900
1930
2000
2030
2100
2130
2200
2230
2300
IMP-8 JUNE 21, 1974

Figure 8

Figure 9 The amplitude, Geocentric Solar Ecliptic longitude, and modulation factor of a type III event detected by IMP 8 on June 10 at 56.2 kHz. Note the very low modulation factor. The exponential decay is very evident in the amplitude plot. The modulation factor is so low at this frequency that the angle shift is caused by the increasing amplitude during the rise portion of the event and the decreasing amplitude during the decay of the event. To get accurate direction-finding measurements the signal must be sufficiently modulated.

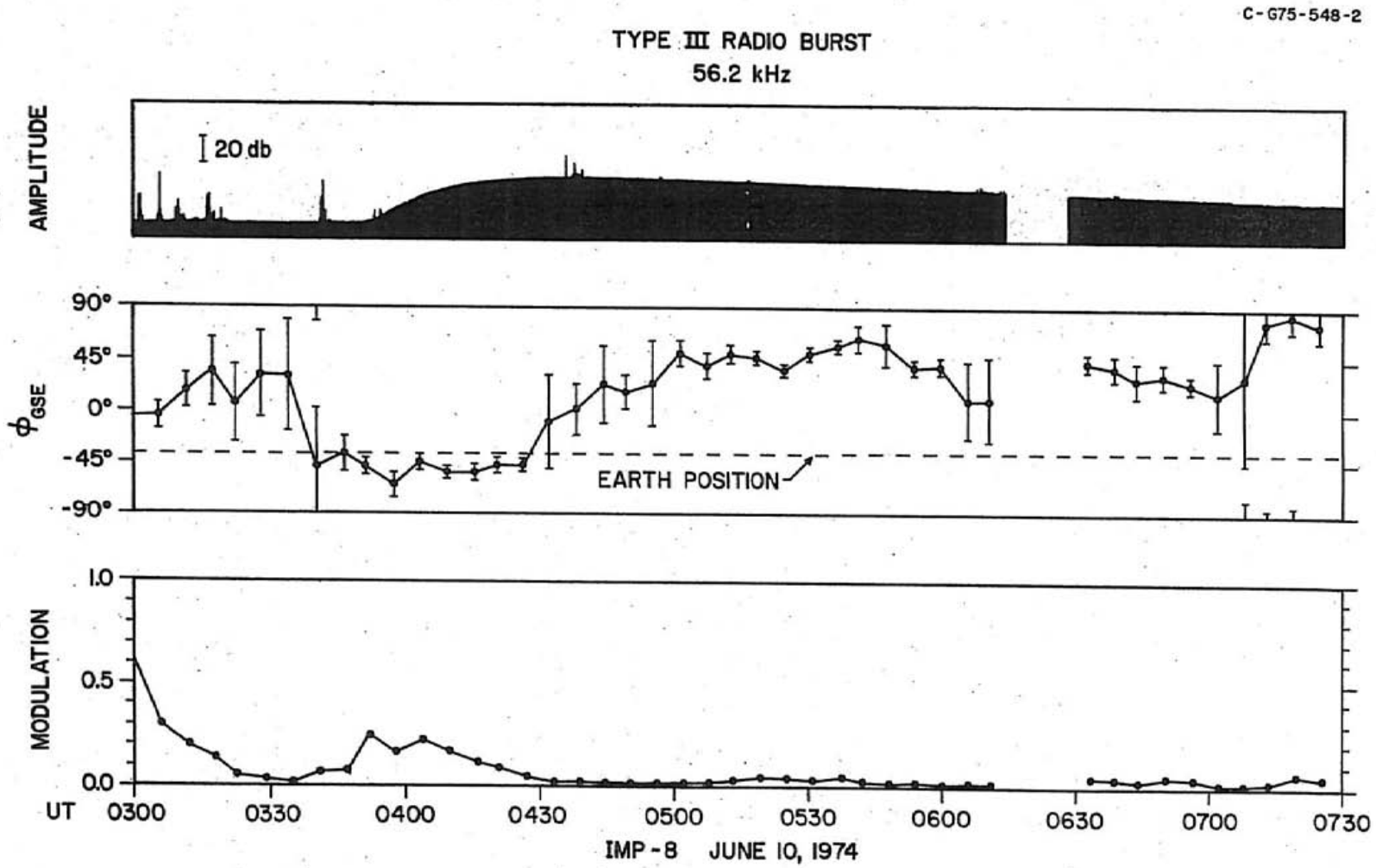
C-G75-548-2
TYPE III RADIO BURST
56.2 kHz
AMPLITUDE
20 db
90°
45°
0°
-45°
-90°
ϕ_{GSE}
EARTH POSITION
1.0
0.5
0.0
MODULATION
UT
0300
0330
0400
0430
0500
0530
0600
0630
0700
0730
IMP-8 JUNE 10, 1974

Figure 9

Figure 10 The RAE emission level scale gives the average radial distance of a type III burst from the sun as a function of frequency of emission. The density scale assumes emission at the second harmonic of the plasma frequency. For one of the events analyzed the RAE emission level scale was adjusted so that the density at 1.0 AU agreed with in situ measurements at 1.0 AU.

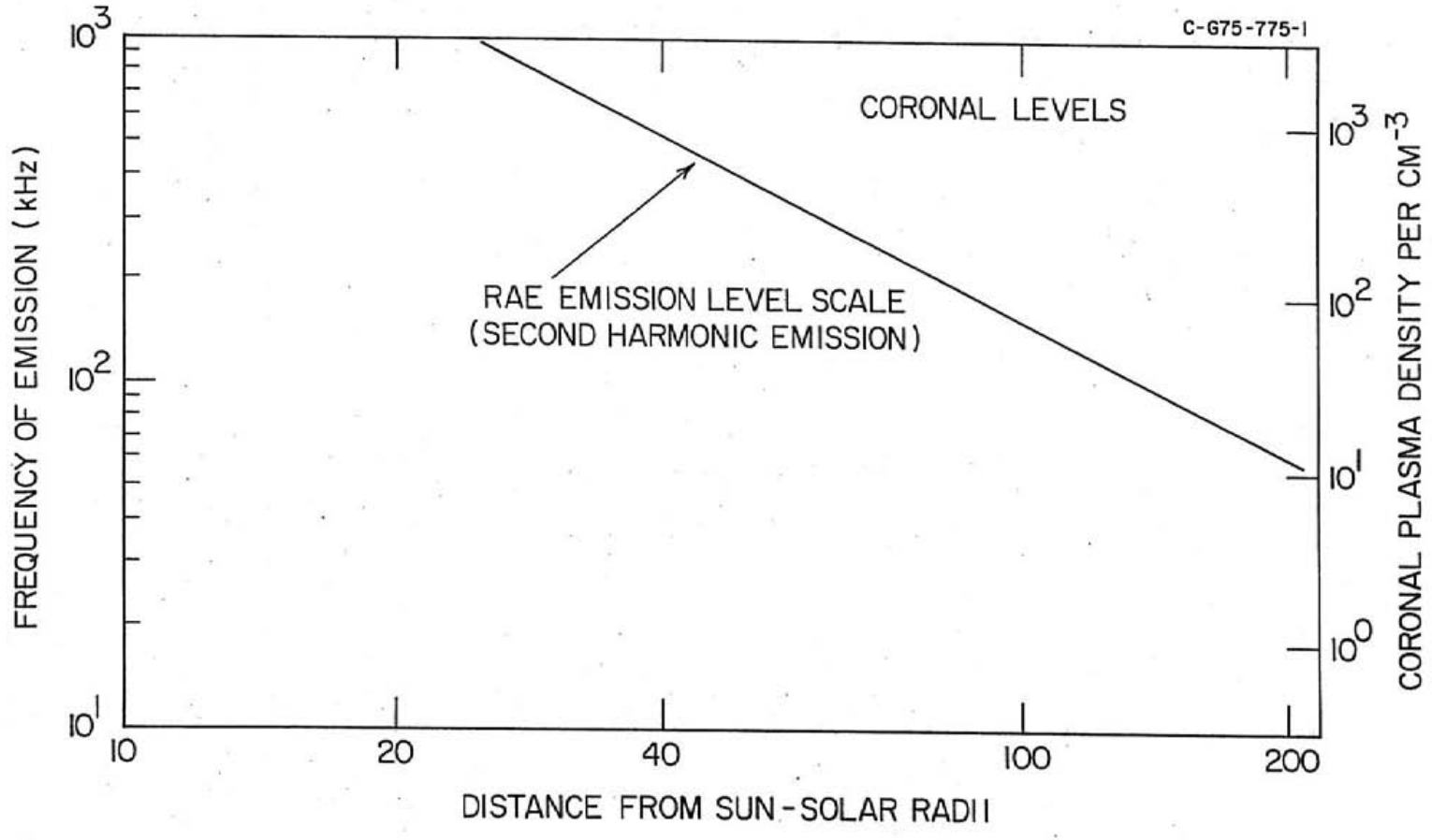
C-G75-775-1
CORONAL LEVELS
RAE EMISSION LEVEL SCALE
(SECOND HARMONIC EMISSION)
FREQUENCY OF EMISSION (kHz)
CORONAL PLASMA DENSITY PER CM-3
DISTANCE FROM SUN - SOLAR RADII
10
20
40
100
200

Figure 10

Figure 11 Three models of the solar magnetic field.

Constant Latitude: Archimedean spirals wound on cones of constant heliocentric latitude. Near the poles the field lines will form a cork screw.

Convergent Field Line Model: Archimedean spiral field lines which extend to lower heliocentric latitude with increasing radial distance.

Divergent Field Line Model: Archimedean spiral field lines which extend to higher heliocentric latitudes with increasing radial distance.

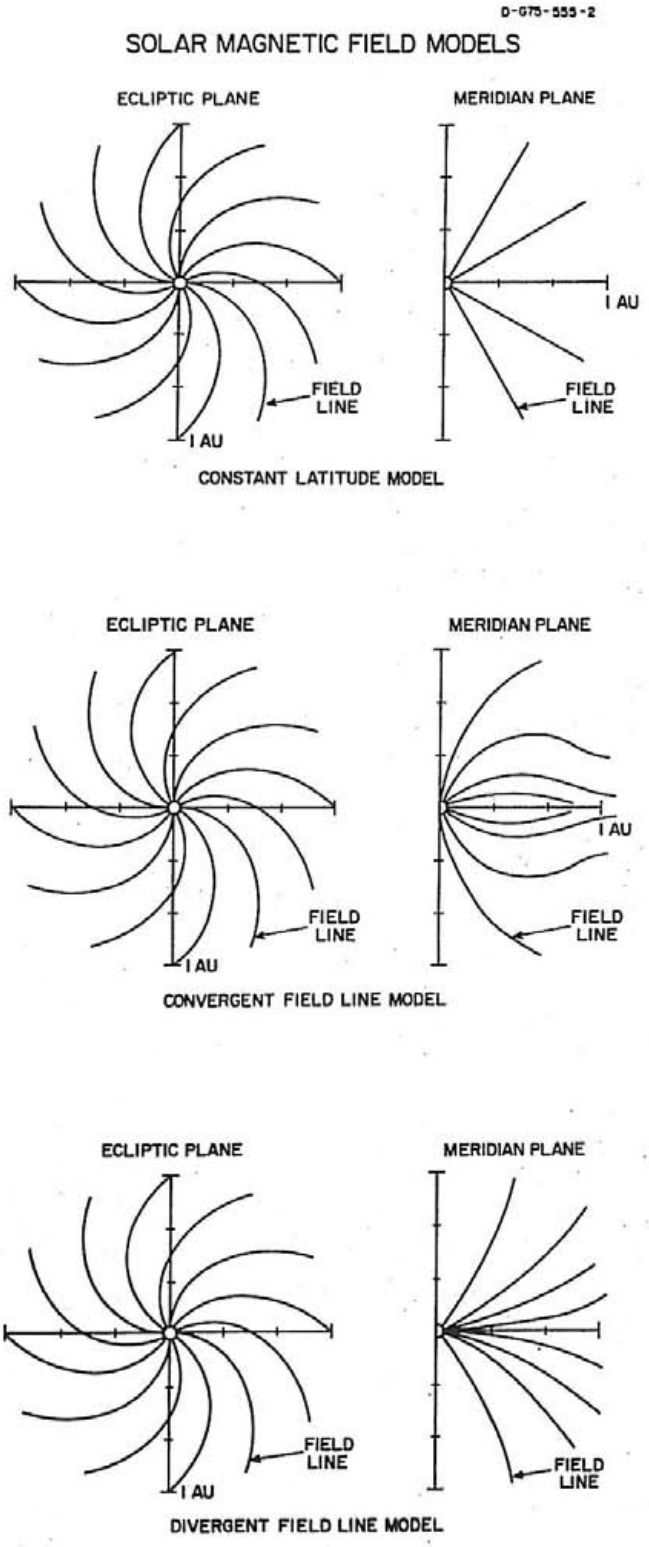
D-G75-555-2
SOLAR MAGNETIC FIELD MODELS
ECLIPTIC PLANE
MERIDIAN PLANE
1 AU
FIELD LINE
1 AU
FIELD LINE
CONSTANT LATITUDE MODEL
ECLIPTIC PLANE
MERIDIAN PLANE
1 AU
FIELD LINE
1 AU
FIELD LINE
CONVERGENT FIELD LINE MODEL
ECLIPTIC PLANE
MERIDIAN PLANE
FIELD LINE
1 AU
FIELD LINE
DIVERGENT FIELD LINE MODEL

Figure 11

Figure 12 Radio direction-finding analysis for the first type III event. The source locations follow an Archimedean spiral configuration in the ecliptic plane. The source locations out of the ecliptic are shown as a function of heliocentric latitude and radial distance from the sun. The bottom panels show the geocentric longitude and latitude predicted by a least squares fit of the constant latitude field line model to the observed geocentric longitudes and latitudes. Note that this event deviates from the constant latitude model for the 56.2 kHz and 42.2 kHz emissions and implies that the magnetic field lines may extend to lower heliocentric latitudes with increasing radial distance. The predicted flare location is found by extrapolating the least squares fit field line back to the sun.

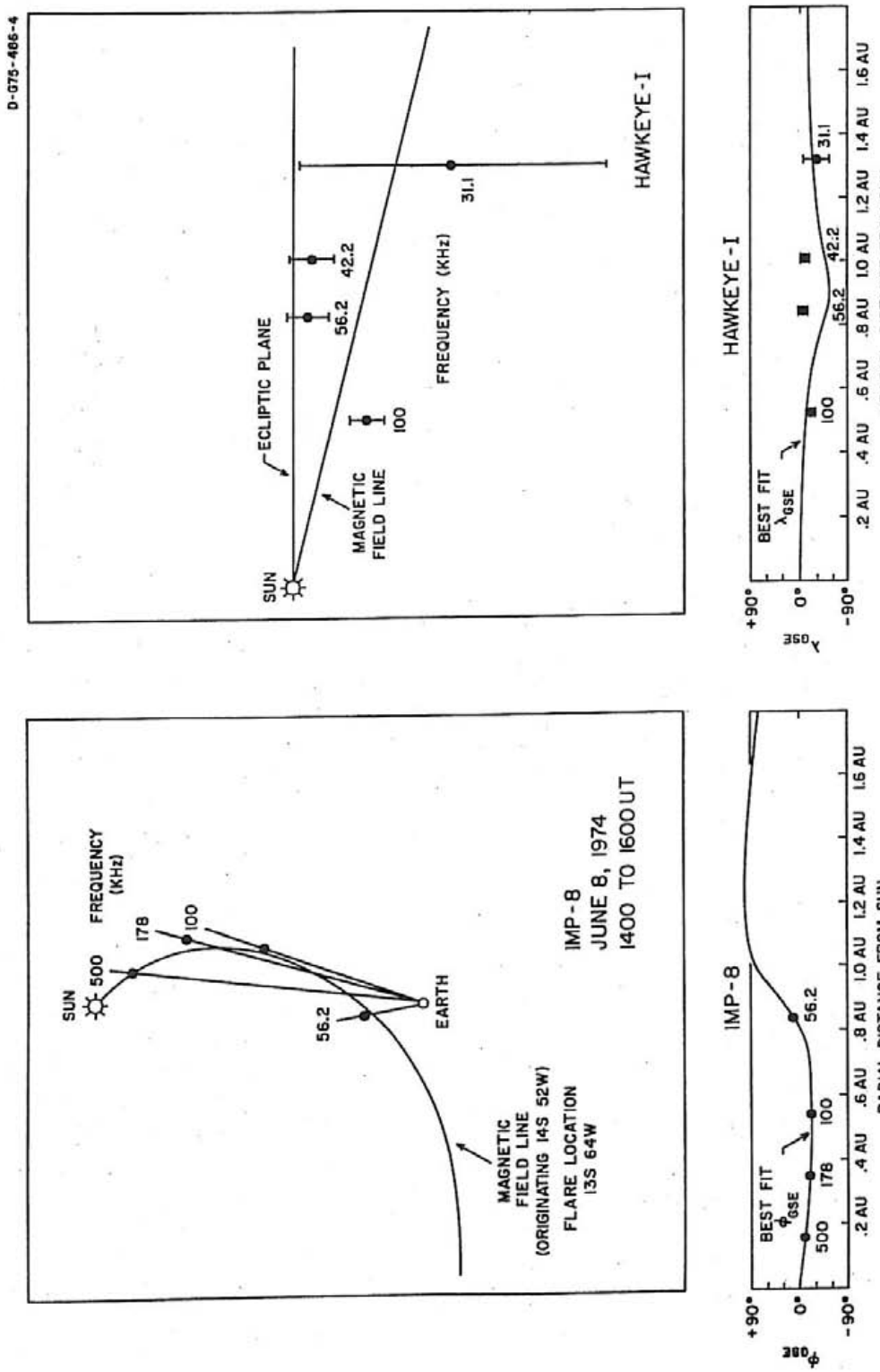
D-675-466-4
SUN
ECLIPTIC PLANE
MAGNETIC FIELD LINE
FREQUENCY (KHz)
100
56.2
42.2
31.1
HAWKEYE-I
SUN
FREQUENCY (KHz)
500
178
100
56.2
EARTH
MAGNETIC FIELD LINE (ORIGINATING 14S 52W)
FLARE LOCATION 13S 64W
IMP-8
JUNE 8, 1974
1400 TO 1600 UT
HAWKEYE-I
BEST FIT
λ_{GSE}
+90°
0°
-90°
.2 AU .4 AU .6 AU .8 AU 1.0 AU 1.2 AU 1.4 AU 1.6 AU
RADIAL DISTANCE FROM SUN
IMP-8
BEST FIT
ϕ_{GSE}
500
178
100
56.2
+90°
0°
-90°
.2 AU .4 AU .6 AU .8 AU 1.0 AU 1.2 AU 1.4 AU 1.6 AU
RADIAL DISTANCE FROM SUN

Figure 12

Figure 13 Direction-finding measurements for another type III event (July 5). Projected into the ecliptic plane the source locations follow an Archimedean spiral configuration. Out of the ecliptic plane the source locations are at nearly constant heliocentric latitudes. Except for the 100 kHz emission the data is consistent with the constant latitude model of the solar magnetic field. Extrapolated back to the sun the least squares fit field line originates near a solar flare.

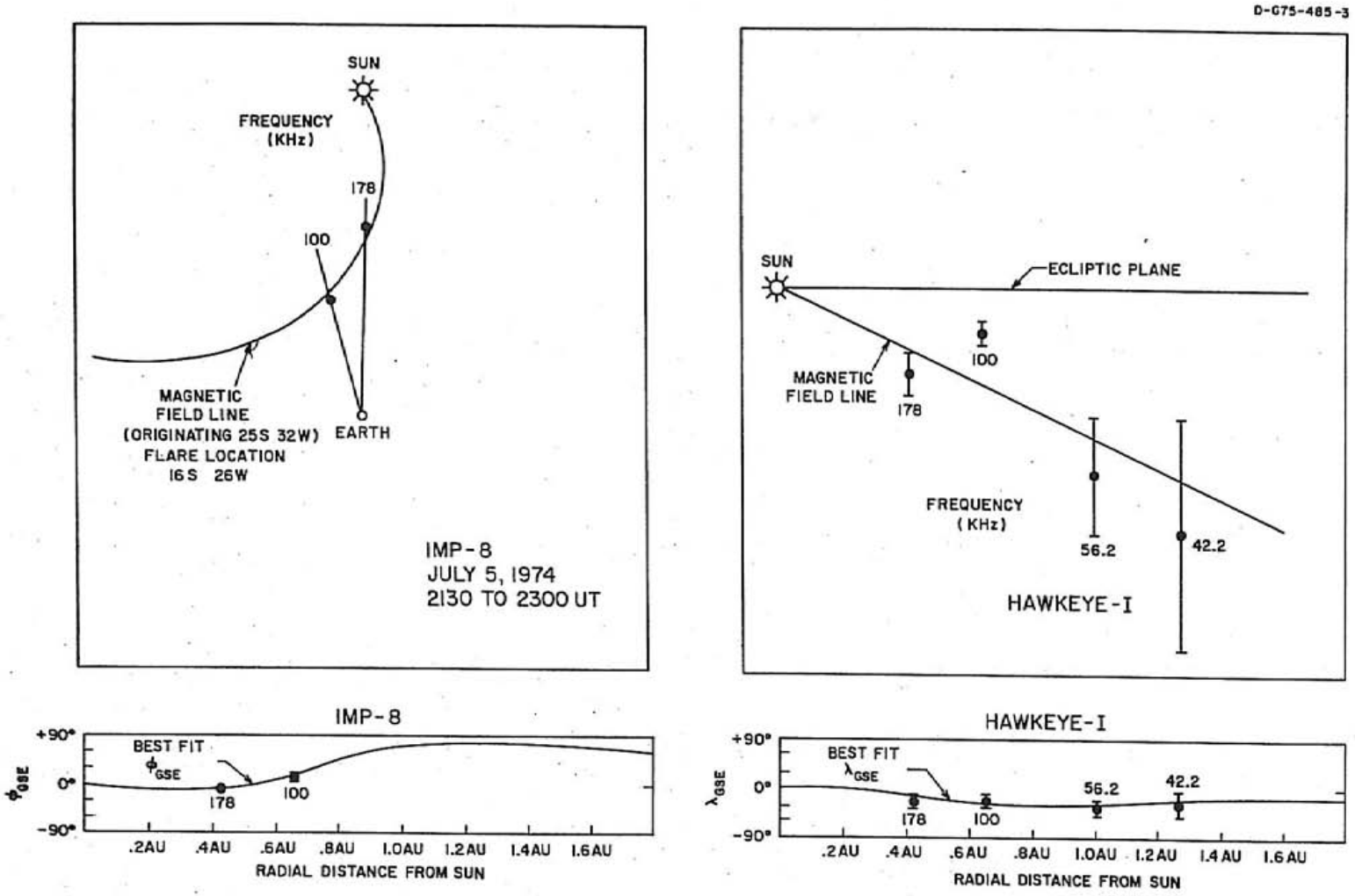
D-G75-485-3
SUN
FREQUENCY
(KHz)
178
100
MAGNETIC
FIELD LINE
(ORIGINATING 25S 32W)
FLARE LOCATION
16S 26W
EARTH
IMP-8
JULY 5, 1974
2130 TO 2300 UT
SUN
ECLIPTIC PLANE
100
MAGNETIC
FIELD LINE
178
FREQUENCY
(KHz)
56.2
42.2
HAWKEYE-I
IMP-8
+90°
0°
-90°
BEST FIT
ϕ_{GSE}
178
100
.2AU
.4AU
.6AU
.8AU
1.0AU
1.2AU
1.4AU
1.6AU
RADIAL DISTANCE FROM SUN
HAWKEYE-I
+90°
0°
-90°
BEST FIT
λ_{GSE}
178
100
56.2
42.2
.2AU
.4AU
.6AU
.8AU
1.0AU
1.2AU
1.4AU
1.6AU
RADIAL DISTANCE FROM SUN

Figure 13

Figure 14 Direction-finding measurements for the third type III event (July 6). Projected into the ecliptic plane the source regions follow an Archimedean spiral configuration. Out of the ecliptic plane the source locations are at a very nearly constant heliocentric latitude, which is excellent agreement with the constant latitude model for the solar magnetic field. Extrapolated back to the sun the least squares fit field line originates near a solar flare.

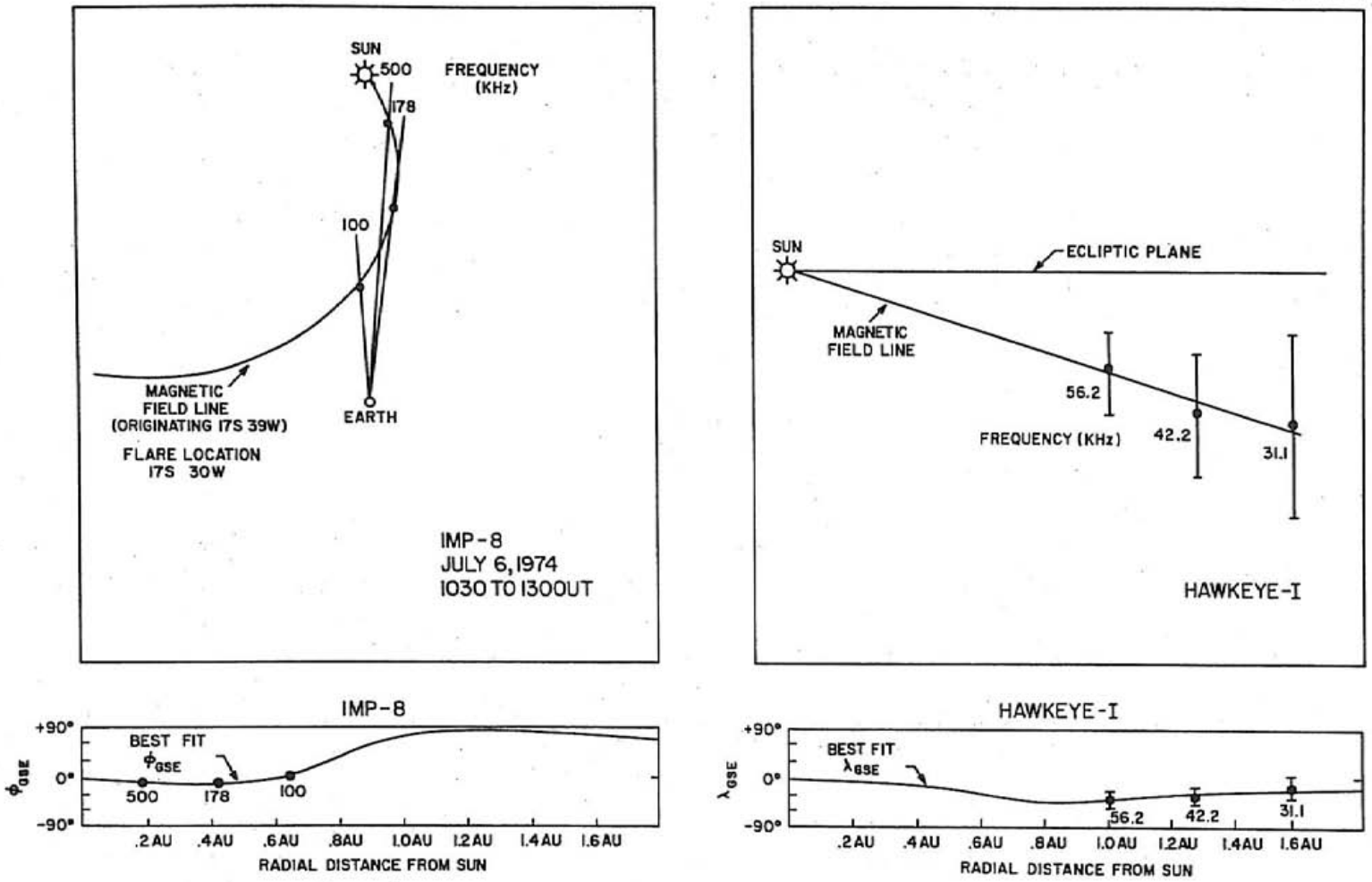
SUN
500
FREQUENCY
(KHz)
178
100
MAGNETIC
FIELD LINE
(ORIGINATING 17S 39W)
FLARE LOCATION
17S 30W
EARTH
IMP-8
JULY 6,1974
1030 TO 1300UT
SUN
ECLIPTIC PLANE
MAGNETIC
FIELD LINE
56.2
42.2
31.1
FREQUENCY (KHz)
HAWKEYE-I
IMP-8
+90°
0°
-90°
BEST FIT
ϕ_{GSE}
500
178
100
.2AU .4AU .6AU .8AU 1.0AU 1.2AU 1.4AU 1.6AU
RADIAL DISTANCE FROM SUN
HAWKEYE-I
+90°
0°
-90°
BEST FIT
λ_{GSE}
56.2
42.2
31.1
.2AU .4AU .6AU .8AU 1.0AU 1.2AU 1.4AU 1.6AU
RADIAL DISTANCE FROM SUN

Figure 14

Figure 15 The modulation factor (index) as a function of half angle source size as viewed from the earth at different elevation angles, α. The source is modeled as a thin, flat disk with each surface element radiating at the same uniform intensity.

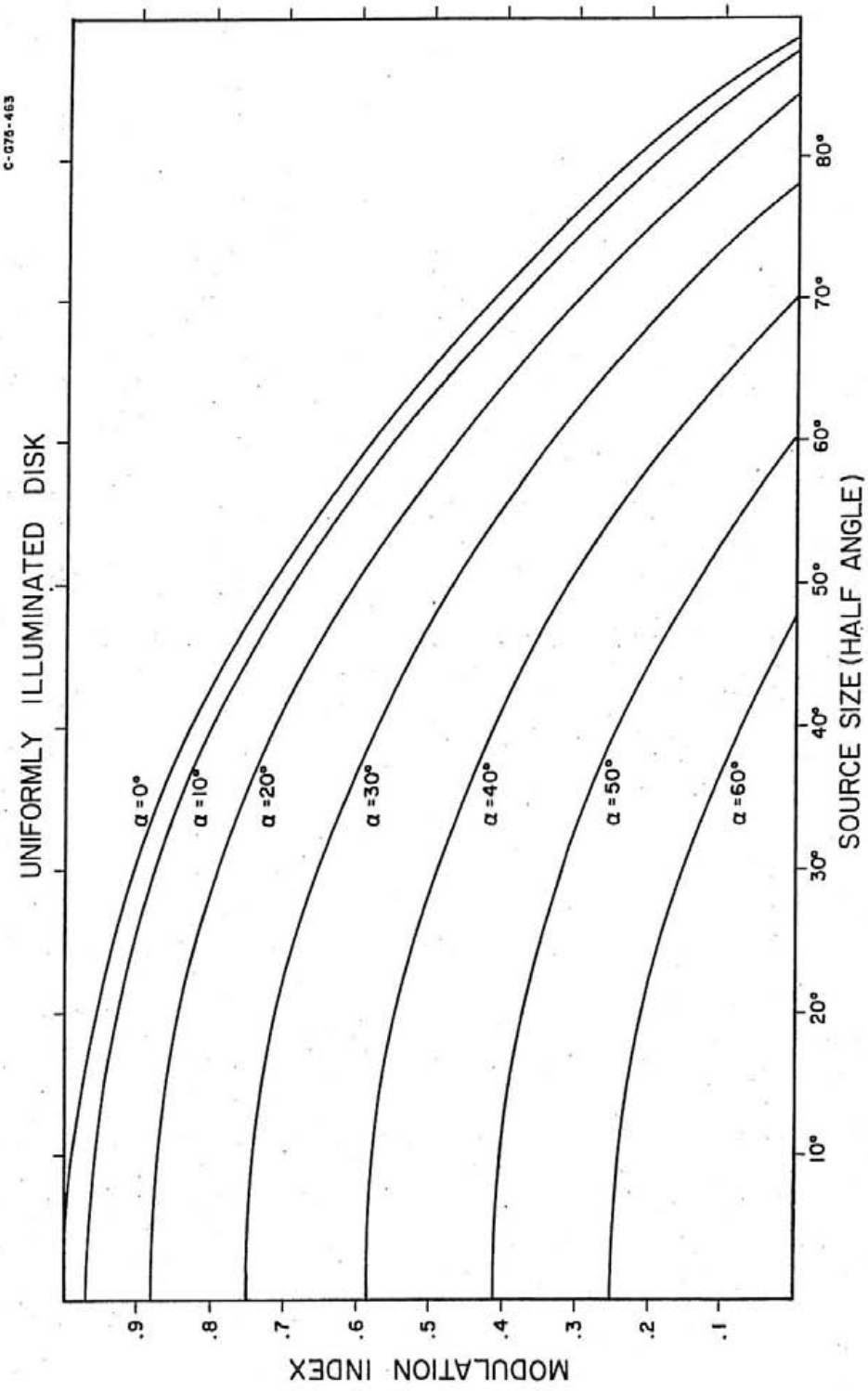
C-675-463
UNIFORMLY ILLUMINATED DISK
MODULATION INDEX
SOURCE SIZE (HALF ANGLE)
α = 0°
α = 10°
α = 20°
α = 30°
α = 40°
α = 50°
α = 60°
.9
.8
.7
.6
.5
.4
.3
.2
.1
10°
20°
30°
40°
50°
60°
70°
80°

Figure 15

Figure 16 The modulation factor (index) as a function of half angle source sizes as viewed from the earth for different elevation angles, α. The source is modeled as a sphere with each volume element radiating at the same intensity. If the satellite is inside of the source the modulation becomes a function of the radial distance from the center of the source divided by the source radius.

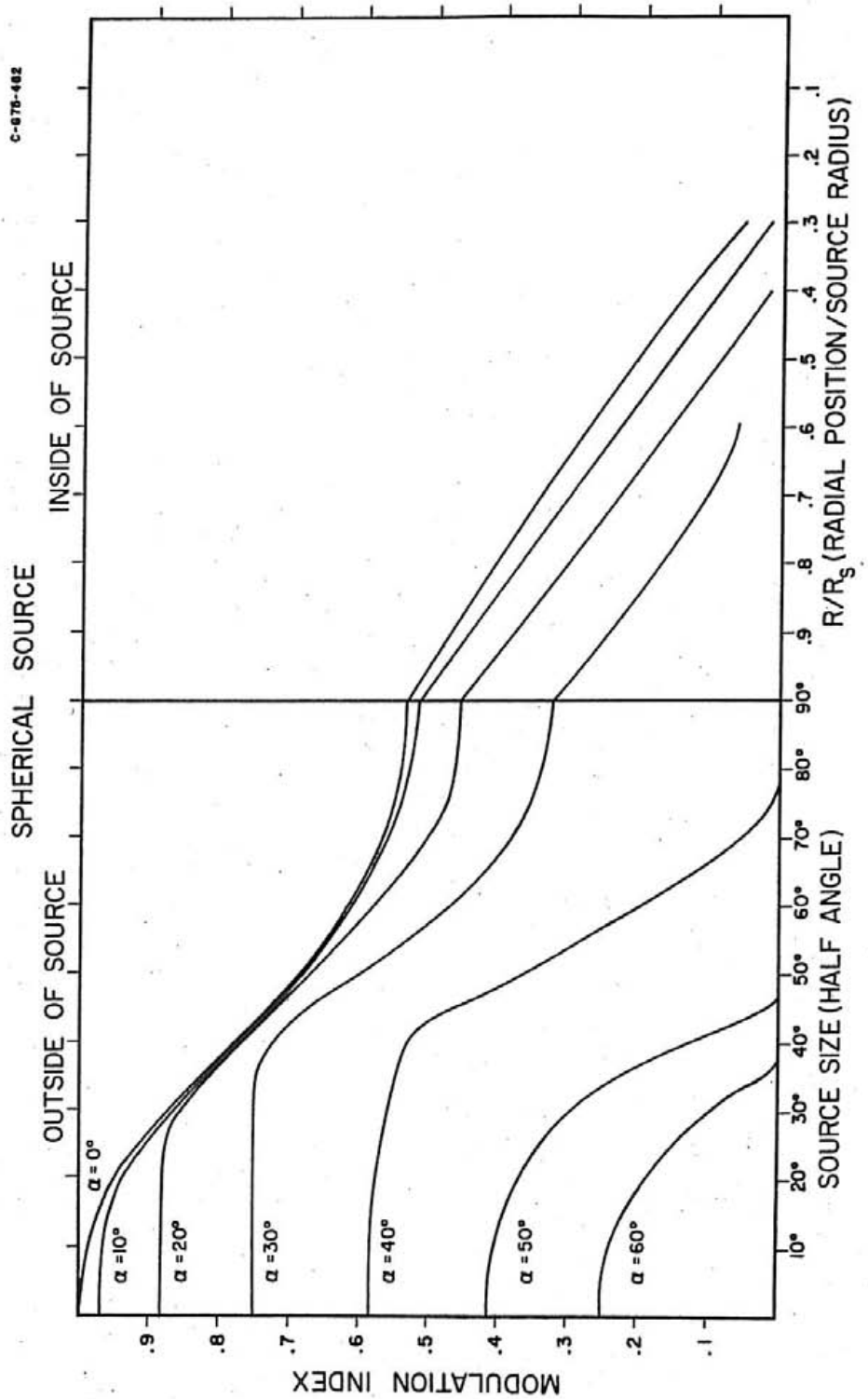
C-678-462
SPHERICAL SOURCE
OUTSIDE OF SOURCE
INSIDE OF SOURCE
α = 0°
α = 10°
α = 20°
α = 30°
α = 40°
α = 50°
α = 60°
MODULATION INDEX
.9
.8
.7
.6
.5
.4
.3
.2
.1
10°
20°
30°
40°
50°
60°
70°
80°
90°
SOURCE SIZE (HALF ANGLE)
.9
.8
.7
.6
.5
.4
.3
.2
.1
R/R_S (RADIAL POSITION/SOURCE RADIUS)

Figure 16

Figure 17 The source size of a type III burst as a function of frequency as seen from the earth, using a thin, flat disk as the modeled source. The frequency of a type III burst is related to the plasma density in the solar wind. As the radial distance from the sun increases the frequency of emission decreases. As the source region gets nearer to the earth the source size increases, as would be expected.

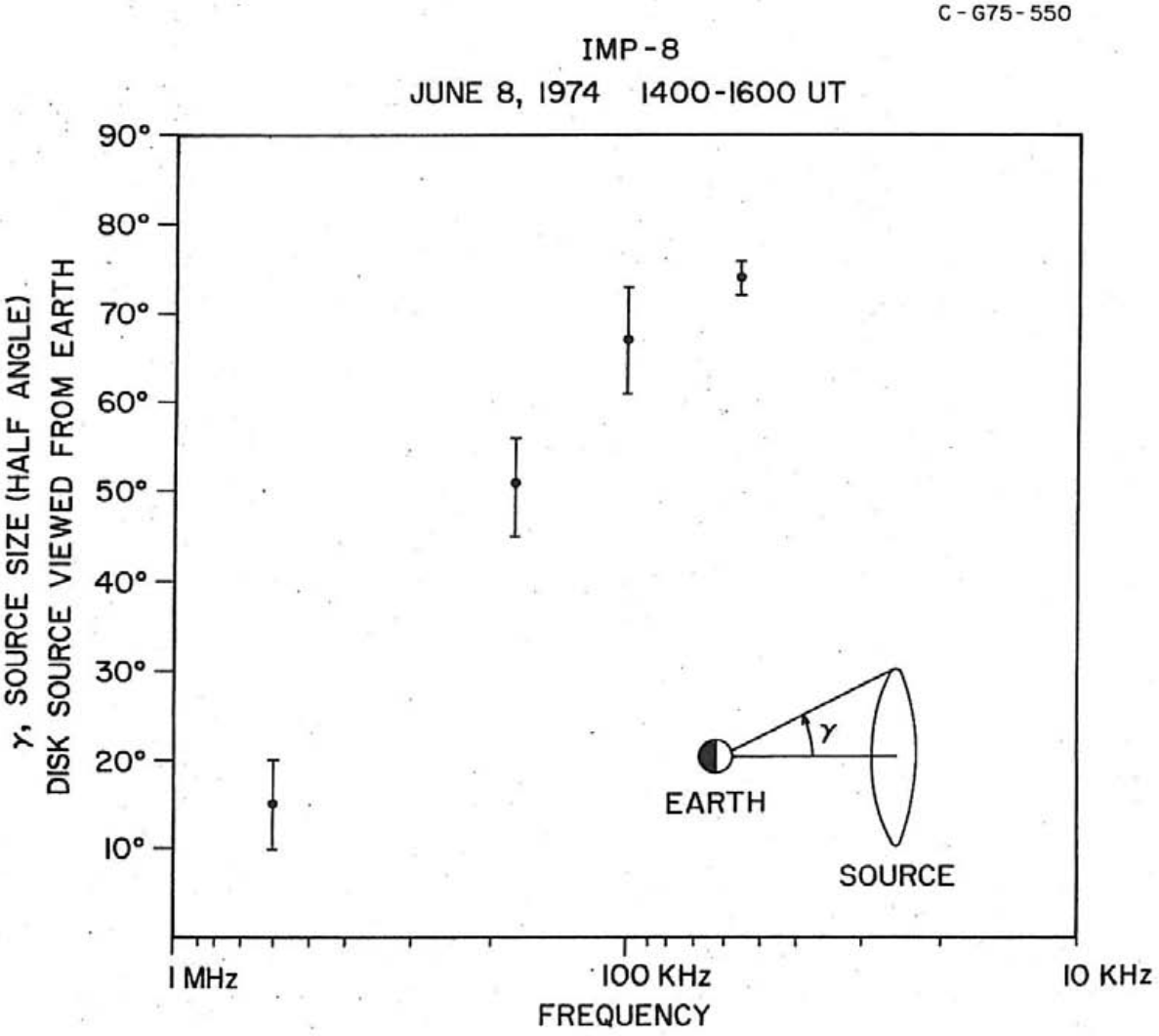
C-G75-550
IMP-8
JUNE 8, 1974 1400-1600 UT
γ, SOURCE SIZE (HALF ANGLE)
DISK SOURCE VIEWED FROM EARTH
90°
80°
70°
60°
50°
40°
30°
20°
10°
γ
EARTH
SOURCE
1 MHz
100 KHz
10 KHz
FREQUENCY

Figure 17

Figure 18 Source sizes as a function of frequency for the same event as in Figure 17 using a source modeled as a thin, flat disk but as viewed from the sun. Note that the source size remains quite constant between the 500 kHz, 178 kHz and the 100 kHz channels. The source sizes are however twice as large as what might be expected from particle measurements.

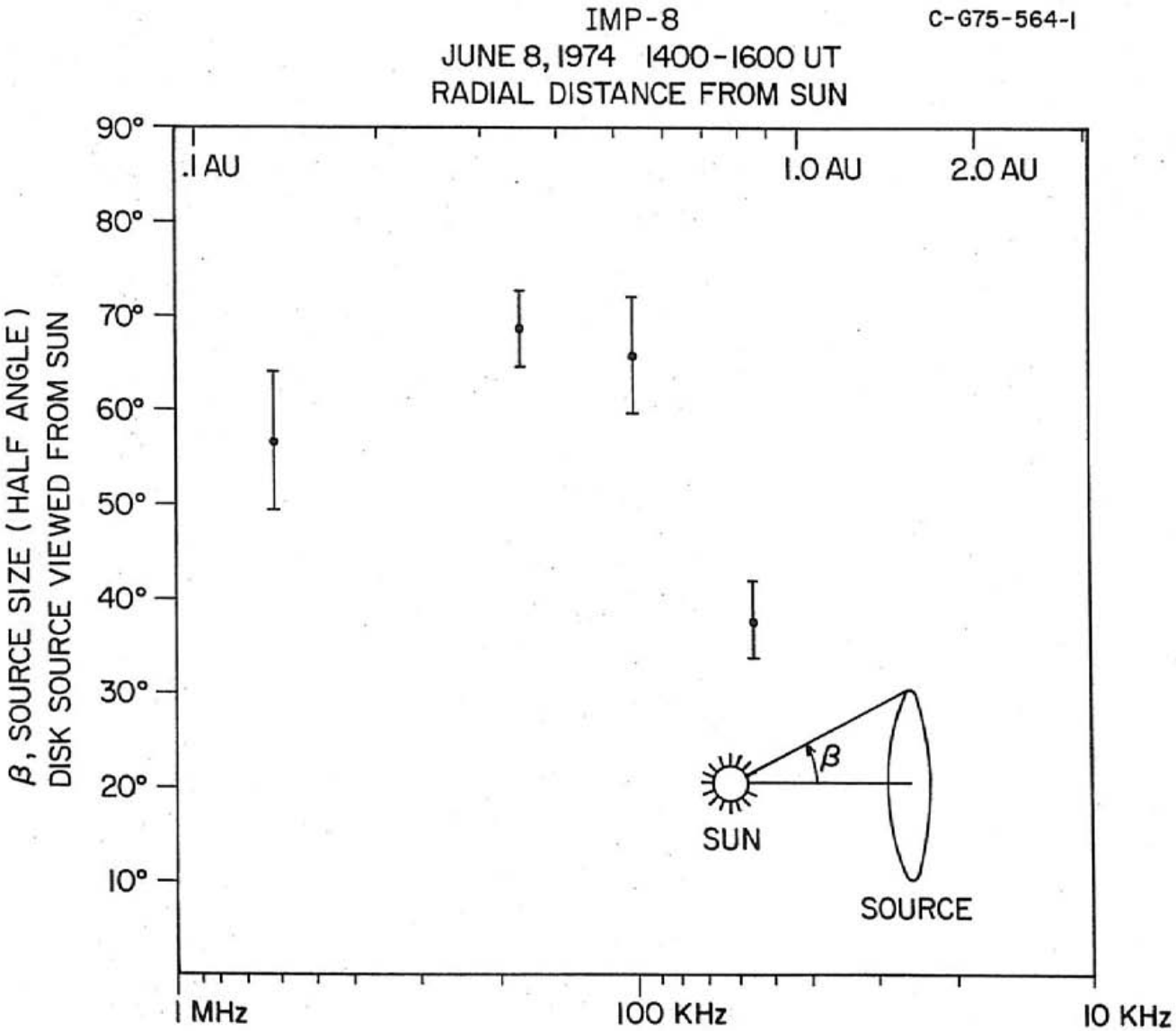
IMP-8
C-G75-564-1
JUNE 8, 1974 1400-1600 UT
RADIAL DISTANCE FROM SUN
.1 AU
1.0 AU
2.0 AU
90°
80°
70°
60°
50°
40°
30°
20°
10°
β, SOURCE SIZE (HALF ANGLE)
DISK SOURCE VIEWED FROM SUN
β
SUN
SOURCE
1 MHz
100 KHz
10 KHz
FREQUENCY

Figure 18